A Study on Self-assembly and Structural Analysis of Protofilaments

by

Divya Jakkam

(Under the Direction of Ramana M. Pidaparti)

Abstract

Microtubules are polymers made of the protein tubulin and play a significant role in various cell functions as they are present in the cytoskeleton of most eukaryotic cells. They have a highly dynamic structure and are formed by the self assembly of the protein tubulin, with the aid of different microtubule associated proteins. Self-assembly is the formation of an organized structure from a series of processes. In this thesis, we seek to observe the formation of a pattern when spherical units which are assumed as tubulins are excited externally by an electrodynamic exciter. The angles of contact which are determined from these experimental results are compared with simulations in virtual reality using a game engine software called Unity. We perform a mechanical structural analysis on the protofilaments, based on the configurations derived from experiments, and study the relationship between different stresses and strains and also, study the variation of stresses relative to the curvature in the protofilament. The mode shapes of these protofilaments are also studied by performing a free-free modal vibrational analysis.

Index words: Microtubules; Self-assembly; Dynamic structures; tubulin; dimer; Protofilament; mode shapes

A Study on Self-assembly and Structural Analysis of Protofilaments

by

Divya Jakkam

B.E., Andhra University, 2014

A Thesis Submitted to the Graduate Faculty

of The University of Georgia in Partial Fulfillment

of the

Requirements for the Degree

Master of Science

Athens, Georgia

2018

A Study on Self-assembly and Structural Analysis of Protofilaments

by

Divya Jakkam

Approved:

Major Professor: Ramana M. Pidaparti

Committee: R. Benjamin Davis
Xianqiao Wang

Electronic Version Approved:

Suzanne Barbour
Dean of the Graduate School
The University of Georgia
December 2018

Acknowledgments

A special thanks to my major professor Dr. Pidaparti, he has been a wonderful mentor through out my research and I have had a great learning experience working with him. I would like to thank Dr. Ben Davis for being a part of my committee and it was his Multiphysics and advanced modeling course which gave me an introduction to research and encouraged me to write research papers. I would also like to thank Dr. Xianqiao Wang for accepting to be a part of my committee and for his invaluable guidance.

I would like to dedicate this thesis to my parents and my brother for all the support they have given me throughout my life and through all the tough times of hardship I had to face. I am indebted to my brother for his immense support and guidance throughout my life. I would like to thank Joshita, Ashwini, Megha and Sanjay for lending me a patient ear and help me bounce ideas with them. I would like to thank my lab mates and friends for all their support.

Table of Contents

List of Figures

List of Tables

Chapter 1

Introduction

Alzheimer's disease and cancer are two of the most researched ailments in the world. The Alzheimer's disease stems from the failure of neurons (nerve cells in the brain), to transmit messages to different organs all across the body [1]. Cancer is caused due to the unmitigated division of cells (called mitosis) which also do not follow apoptosis which is the programmed cell death [2].

The common point in either of these diseases is the failure in the working of the cells. These ailings are directly caused due to the malfunctioning of the human cell either because of their untimely death or unconstrained proliferation of cells. Alzheimer's is believed to occur either because of the build-up of proteins like the tau protein, which cause aggregates in cells and prevent them from executing their jobs, or the premature death of healthy cells. The tau protein which should associate with microtubules instead links itself to another tau protein, thereby culminating in the formation of tangles and causing rapid severing of microtubules in the nerve cells [3]. In cancer, the tubulin protein that makes up microtubules is found to be slightly altered [4], which promotes mitosis, further instigating the formation of tumors.

Here, the main focus is on the role of microtubules in these and other diseases pertaining to cells. Due to the microtubules being living, dynamic structures within the human cell measuring up to a maximum of a couple of microns in length, studying them *in vivo* is an expensive affair. The structure of microtubules vastly determines its functionality, causing many researchers to focus on developing a computational model. We are pursuing the possibility of developing such a model by observing self assembly in microtubules - which is

how the microtubules develop within the cell. We also seek to perform structural analysis on the microtubule system by using a bottom up approach, to know more about their response to different stresses applied on them. The stress-strain relationships for the protofilaments structure are obtained so it could be used to present a predictive model that could be utilized, instead of *in vivo* studies, thereby providing a cost-effective way for further research.

Self-assembly is the process in which particles in nature organize themselves into simple or complicated structures [5]. In nature, self assembly seems ubiquitous as it can be seen in the gathering of swarms of bees, schools of fish in the ocean and flock of birds in the sky [6]. In nature, this process is a means to make itself a stronger unit relative to its weaker form when considered as individual units. On assembly, the structures formed are complex with the ability to carry out higher order functions. Self-assembly of biomolecules into extended structures is very common and provides crucial functions [7]. A perfect example of naturally self-assembled structures are microtubules. These structures are dynamically self-assembled nano-scale structures. Microtubules form an intrinsic part of the cytoskeleton of eukaryotic cells and are responsible for maintaining the structure of the cytoskeleton.

The rest of this document is organized as follows: Chapter 2 provides an introduction to the topic, providing necessary definitions and information required for understanding the concepts used in this thesis. A general introduction to previous investigations on the mechanical behavior of microtubules and their structure is listed, along with a summary of prior studies on the mimicking of self assembly in microtubules and their structural analysis. A brief overview of the existing instances of self-assembly and various models showcasing self-assembly and the applications of self assembly concepts on microtubules is provided in this chapter. In Chapter 3, the experiments performed on the electrodynamic exciter to observe self assembly in microtubules are discussed, starting with protofilaments. The experimental data are compared with simulation results obtained from the game engine, Unity. In Chapter 4, we study the strength analysis of the structure of a protofilament, applying the configurations obtained from the results in Chapter 3. We also explore the

mode shapes which result due to a free vibrational analysis of the protofilament structure. Chapter 5 provides discussions and conclusions drawn from this study, along with future work.

Chapter 2

Background

Before we get into the specifics of this thesis, we provide a groundwork by explaining the pre-requisites and terms used. Organisms are generally made up of a group of organs which perform specific functions. The organs are, in turn, a collection of tissues which are made up of cells. Figure 2.1 shows the structural organization hierarchy maintained in the human body.

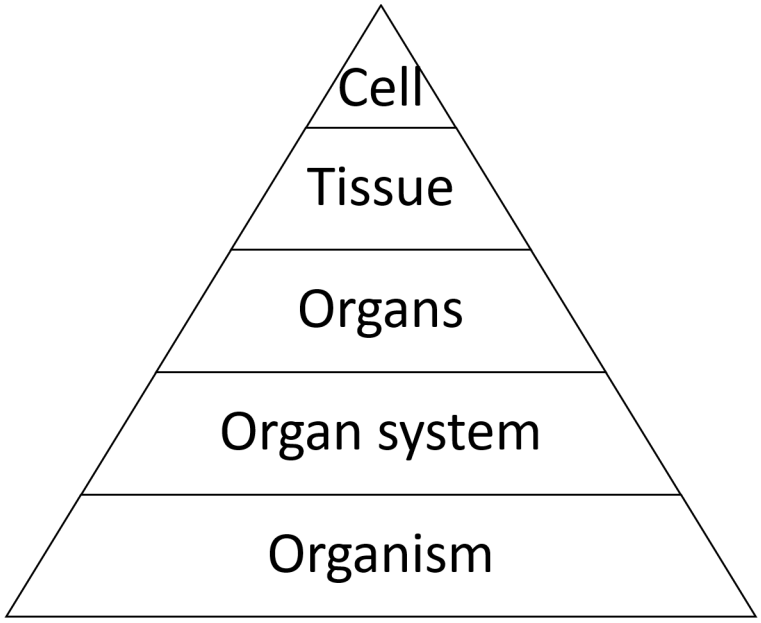

Figure 2.1: Structural organization levels in an organism

2.1 Cells - History

Cells are the basic unit of life and can be referred to as building blocks of the structure of any living organism. They are responsible for all the metabolic processes within a living organism.

They are broadly divided into two main classes: 1) the Prokaryotic cells and 2) the Eukaryotic Cells. Prokaryotic cells are small, simple cells which lack a nucleus and are generally bacteria. The Eukaryotic cells are more complex, due to their having a nucleus, cytoskeleton, cytoplasmic organelles. They are most commonly found in yeast, plants, animals, and human beings. The cytoskeleton is a grid of proteinous filaments which are found in the cytoplasm and are responsible for maintaining the cell shape and overall structural framework of the cell. The cytoskeleton contains a network of filaments which enables it to perform these vital functions. These filaments have been identified as actin filaments, intermediate filaments and microtubules. Actin filaments control the shape of the cell, microtubules help in cell division, and the intermediate filaments form the skeleton of the cell, thereby, giving it elastic and tensile characteristics [8]. A representation of a Eukaryotic cell and its components are shown in the Fig. 2.2.

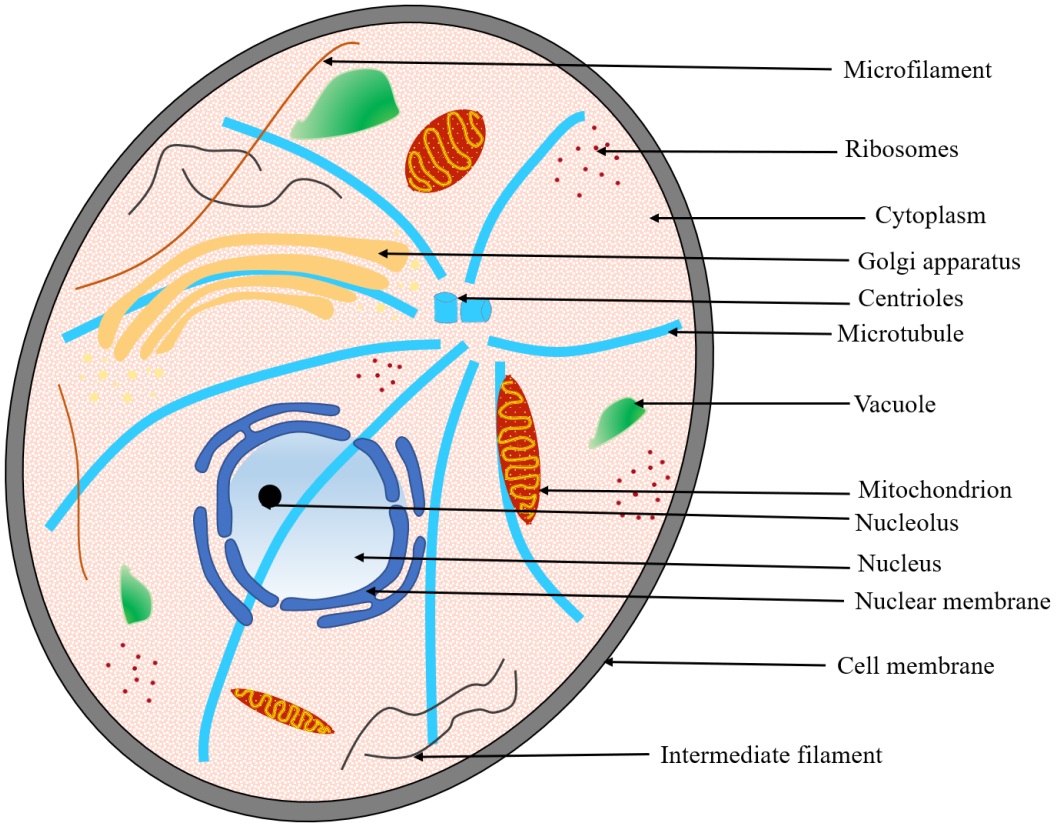

Figure 2.2: Structure of an animal cell

2.2 Microtubules

Microtubules (MTs) are one of the three principal fibrous components found in the cytoskeleton of a living eukaryotic cell. Because of their tubular configuration, they have a stiffer structure compared to the two other cytoskeletal fibers, the microfilaments and the intermediate filaments.

The microtubule has a hollow, cylindrical rod-like structure which is made up of heterodimers of tubulin. As explained earlier, monomers of α-tubulin and β-tubulin bond to form a heterodimer. These monomers are each about 4nm in diameter, making the heterodimer about 8nm in length. When these dimer subunits join end-to-end longitudinally, they form protofilaments which further come together to form tubular rings. They have a dynamic structure which continually undergoes rapid assembly and disassembly within the cell due to the hydrolysis of GTP and interaction with other microtubule associated proteins (MAPs).

According to Kirschner and Mitchison [9], three types of microtubules help in the formation of the mitotic spindle, which are:

1. Kinetochore microtubules, found in the mitotic spindle
2. Polar microtubules, also found in the mitotic spindle
3. Astral microtubules, which protrude from the centrosomes to the periphery of the cell

Functions of microtubules

Because of their highly dynamic structure, which continually undergoes self assembly and disassembly, they are responsible for some vital functionalities within the cell, some of which are:

1. Organizing and maintaining cell shape
2. Intracellular transport

3. Movement of organelles in the cell

4. Cell division in mitosis

5. Beating of cilia and flagella

Structure of a microtubule

Microtubules are made of different configurations based on the number of protofilaments, but the most common of them is the 13-3 configuration. This architecture consists of 13 linear protofilaments which are laterally bound with a helical start number of 3, thereby forming a tubular spiral structure [10]. MTs can measure upto a length of several nanometers to a few microns.

Catastrophe and Rescue

It has already been mentioned that microtubules have a very dynamic structure which involves rapid assembling and disassembling states, which is referred to as dynamic instability. *Catastrophe* is the state at which the microtubules undergo deploymerization, resulting in the shortening of the MT length. When the microtubule structure undergoes an increase in its length due to the polymerization of tubulin dimers, this process is referred to as *rescue*.

2.3 Tubulin

Tubulin is a family of proteins which are the major components of microtubules, commonly found in Eukaryotic cells. There are ongoing studies which are researching tubulin-related proteins (TubZs) in Prokaryotic cells as well [11].

In eukaryotes, the tubulin super family has six members, which are listed below:

1. α - tubulin

2. β - tubulin

3. γ - tubulin

4. δ - tubulin

5. ϵ - tubulin

6. ζ - tubulin

The α-, β- and the γ- tubulins are the most pervasive members of the tubulin family to be present in all eukaryotic organisms. The α- and β- tubulin monomers are the ones which are responsible for polymerization into dimers, which would subsequently aid in the formation of microtubules. The γ - tubulins which are found in the microtubule organizing centers (MTOCs) help initiate the formation of microtubules [12]. It is observed that δ - tubulin links longitudinally with α - tubulin, at the minus (-) end of the microtubules, while the ϵ - tubulin interacts with the plus end of the β - tubulin [13].

Tubulin dimer

The tubulin dimer can be referred to as the building block of the microtubule structure. The α- and β- tubulins polymerize and link together to form a tubulin heterodimer. These heterodimers chemically bind with each other in the longitudinal direction to form protofilaments. This tubulin subunit is created on interaction with GTP (Guanosine triphosphate) molecules and form strong bonds which do not dissociate easily [14]. According to Lodish, the lateral and longitudinal interactions between tubulin subunits aids the formations of microtubules. Longitudinal interactions lead to the development of long protofilaments, while lateral interactions between dimers assist in the organization of sheet or ring-like structures.

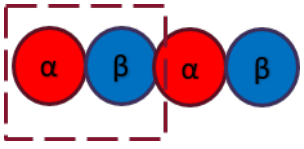

Figure 2.3: Tubulin dimers

As can be seen from Figure 2.3, the dimers are arranged from head-to-tail in a protofilament. This means that one end of the protofilament contains the α - tubulin, while the opposite end of the protofilament contains the β - tubulin. This kind of alignment creates a polarity in the resulting structure.

2.4 Microtubule-associated Proteins

Microtubule associated proteins are referred to as the MAPs. The function of these MAPs is to regulate the assembly or disassembly of microtubules and aid in maintaining the stability of the MT structure. They affect the lengths to which a microtubule could either grow or shorten. They also help link the microtubules to other organic components like membranes or protein complexes. Some of the MAPs are tau, EB1, MAP1, MAP2, MAP4 and +TIP. The linking of microtubules with different MAPs gives rise to the microtubules' ability to perform different functions.

2.5 Microtubule Motor Proteins

Microtubule motor proteins move across the microtubules and enable them to perform intracellular transport and various other cell movements. Based on the direction of movement along the microtubule, they can be classified into plus end motors and minus end motors.

The two major classes of proteins responsible for this function are Kinesin and Dynein. They utilize the energy derived from the hydrolysis of ATP to help walk along the microtubule. Dynein moves along towards the minus end and Kinesin walks over to the plus end of the microtubule. They are specifically responsible for the intracellular transport, positioning of membrane vesicles and organelles, separation of chromosomes at mitosis, and beating of cilia and flagella [15].

Cassimeris, et al., performed simulations to model an array of dynamic microtubules using a Monte Carlo method. Their algorithm calculated the average microtubule lengths and stability of MTs and the factors that affect these properties [16]. From the experiments conducted by Lenz and Whitten [17], they believed that self assembled matter could be studied by using new design principles where geometrical units form into aggregates on excitation. Papadopoulou, et al. designed self replicating spheres to explore the cellular growth and division in a macro scale, using non-robotic components and non biological material. They placed magnets internally in the spheres to allow them to connect and disconnect with neighboring units thereby promoting cell mitosis [18].

Motamedi and Mashhadi studied the bond interactions within each of the tubulin dimers using Molecular Dynamics (MD) simulations, and determined the Young's modulus and other mechanical properties of the MTs using a finite element model [19]. They assumed each tubulin monomer to be a sphere with a nonlinear spring connecting them to achieve their results. Kasas et al., used a finite element model [20] assuming tubulin dimensions from Chretien and Wade [10] to determine the mechanical properties. α- and β- tubulins were assumed to be the same, structurally for their model. Civalek and Demir proposed a nonlocal finite element model based on the Euler-Bernoulli beam model to analyze the effect of buckling on MTs [21]. They applied the Winkler spring model to the elastic matrix surrounding the microtubule and noticed an increase in the buckling loads with an increase in the elastic matrix parameter. The GTP cap at the end of the MT helps in maintaining the stability of the MT structure as the GTP bound tubulin helps in polymerization and arrests catastrophe [9]. It has been observed that protofilaments with GDP (Guanosine diphosphate) linked tubulins at the ends have an intrinsic curvature. Janosi, et al proposed that this slight bending of the protofilament at the ends allows in the release of some built-in stress [22].

Kis et al. investigated the anisotropic properties of MTs by using an AFM (Atomic force microscope) on a perforated surface [23]. They believed that the protofilaments of an MT are

analogous to ropes of single walled carbon nanotubes and determined a relation between the Young's modulus and shear modulus. Experiments were conducted by Shi et al., on a single microtubule where they observed the link between flexural rigidity and the MT length using a laser trapping technique and dark-field microscopy [24]. An atomic resolution model of an MT was built to determine stress-strain dependence on extension and compression, thereby obtaining values of the Young's modulus which was comparable to previously published data [25]. A coarse-grained model of the MT was developed to study the mechanical properties of the MTs by assuming different types of lateral bonding between adjacent protofilaments [26]. Nogales et al. conducted electron crystallography studies to observe the structure of the dimer formed by α- and β- tubulins and determined that teir structures are nearly identical and compact [27]. Donhauser et al. developed a finite element model to evaluate the effect of radial deformation on various MT types and found that the orientation of the protofilament does not have any effect on the radial stiffness of the MT [28].

Chapter 3

Protofilament self-assembly: Experiments and Simulations

Self assembly is the process in which a system undergoes various interactions within the system to form an orderly state. It is a very prevalent aspect in most distributed systems like physical, chemical, biological, robotic and cognitive systems. Studying this theory of self organization provides a way to understand the emergence of order in the universe, by providing simple rules which specify the interactions at a cellular level. When these elementary level interactions result in a pattern formation at the macro level, we gain an understanding of the workings of the process of emergence whereby new levels of organization are created. The Self-Assembly Lab at MIT experimented with self replicating spheres where they explored macro-scale cell mitosis, with the help of magnetic fields and an agitating table to facilitate cell movement, growth and division [18].

The formation of the microtubule structure is a result of the self assembly of the different elements (like proteins), present inside the cell, due to local interactions within the Eukaryotic cell. We designed experiments to observe this self assembly by using the attractive and repulsive forces provided by a magnetic field. The experimental set-up, shown in Fig. 3.1, consists of an enclosure mounted on an electrodynamic exciter which produces vibrations, which in turn are, transmitted to the spherical units contained within the enclosure. On excitation, these units interact with each other to form structures which will be examined later on in this chapter.

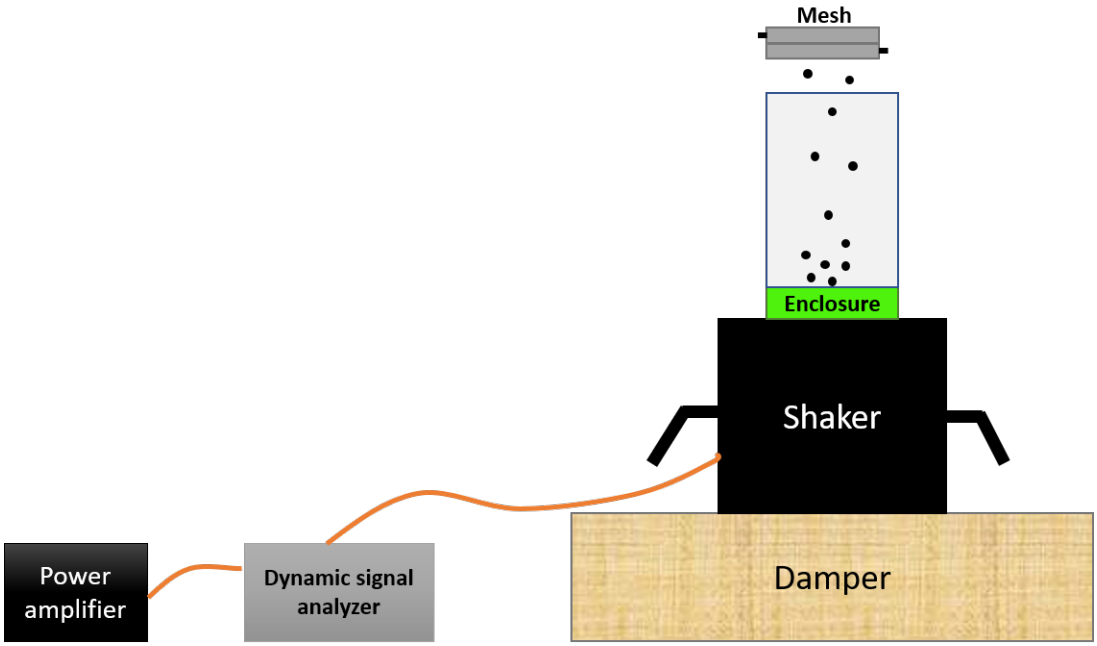

Figure 3.1: Experimental set-up

3.1 Vibration shaker

The vibration source which provides input to the set-up is an electrodynamic exciter. An electrodynamic exciter or shaker is a device which is used for vibrational or modal testing, by creating an environment in which the components to be tested are mounted on the shaker's head. The endurance of the component is observed by varying the frequency at which the set-up is made to vibrate. The exciter used in our experiments can provide up to 40 lbf pk sine force[1] and is ideally used for vibration control testing of components and self-assemblies.

The shaker is used in tandem with a power amplifier and a function generator through which the frequency and amplitude can be input into the system. The values of the frequency are varied while the amplitude is maintained at a set value. It has been observed that the rate of formation of structures increases on increasing the gain to the system. Similarly, an increase in the frequency results in an increase in the excitation to the system as well. It

[1] A sinusoidal force of 40 pounds for a sine test

can be observed from the experiments, that the best way to get a varied range of vibration outputs is by regulating either the gain or the frequency.

3.2 Enclosure

The enclosure consists of a circular platform which is fastened on to the top of the shaker's head and a plastic sheet which is wrapped around the base and serves as a wall to enclose the units within it. The platform is secured to the shaker with the help of steel screws. The platform was modeled in AutoDesk Inventor keeping in mind the dimensions of the shaker head, and then 3D printed so that it fits perfectly on the shaker. The base of the platform was made with plexiglass and the interesting fact about this material is that, it provides enough bounciness in the units which accounts for a highly excited movement within the enclosure.

Figure 3.2: Platform

3.3 Vibration Damper

A vibration damper is a device or a material which is used to absorb any unwanted vibrations or noise. In our experiments, a thick foam padding is used which works effectively to isolate our system.

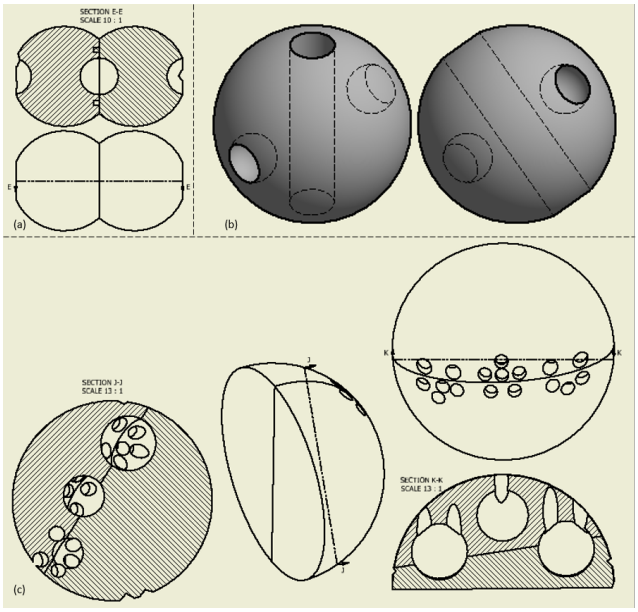

Figure 3.3: Different designs considered for mimicking the dimer unit: (a) Each end of a unit holds a single magnet which lets them bond with other units to form straight chains; (b) Similar to (a), but is lighter as it uses less material during 3D printing because of the cylindrical void; (c) Contains three magnets in each unit with vents to allow for the magnetic field to spread out, thereby attracting other units which results in chains

3.4 Development of the experimental model

Tubulin dimers measure approximately upto 8nm in length [29] and consists of both the α and β tubulins bonded within. Because of the nano scale size of the dimers and their near circular contour, we have assumed our units to be spherical in shape for ease of experiments. It is known that microtubules are highly dynamic structures, and hence the units should easily be able to associate and disassociate with each other. We exploited the effects of a magnetic field for this purpose and used small spherical magnets inside the units. The spherical units [30] were modeled in AutoDesk Inventor as in Fig. 3.4, and then 3D printed by preparing the models in Preform software. After designing several models and testing them, we finalized on the design shown in Fig. 3.5. Considering the diameter of the spherical magnets, this model has been designed so that it can hold upto six magnets without any interactions from within the unit itself. This design has been finalized after many trial and error attempts as shown in Fig. 3.3.

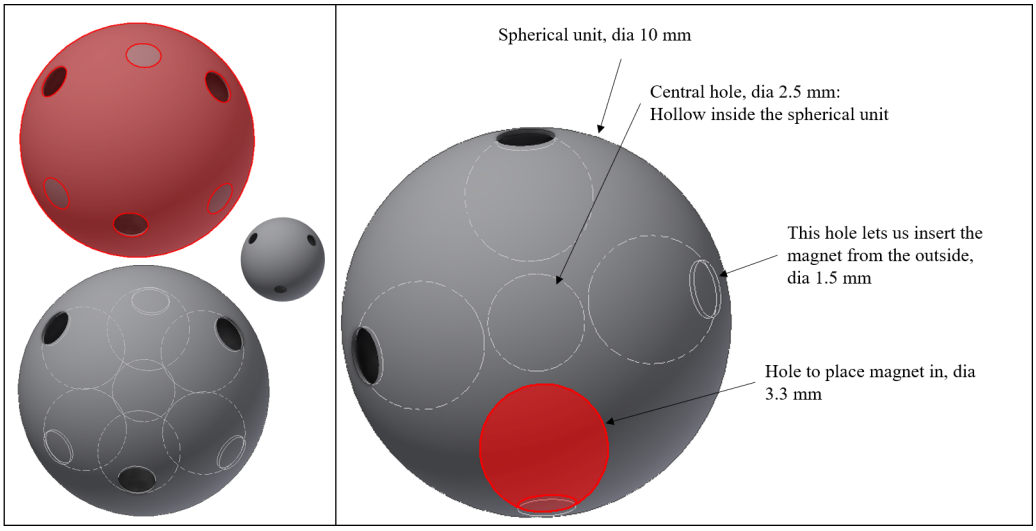

Figure 3.4: Design of the experimental model

Fig. 3.5 shows the outline of the design we have used for our experiments. This design has been finalized as it could be used to form filaments when there are two magnets in each unit, sheets when there are four magnets in each unit, and tubules when there are six magnets in each unit.

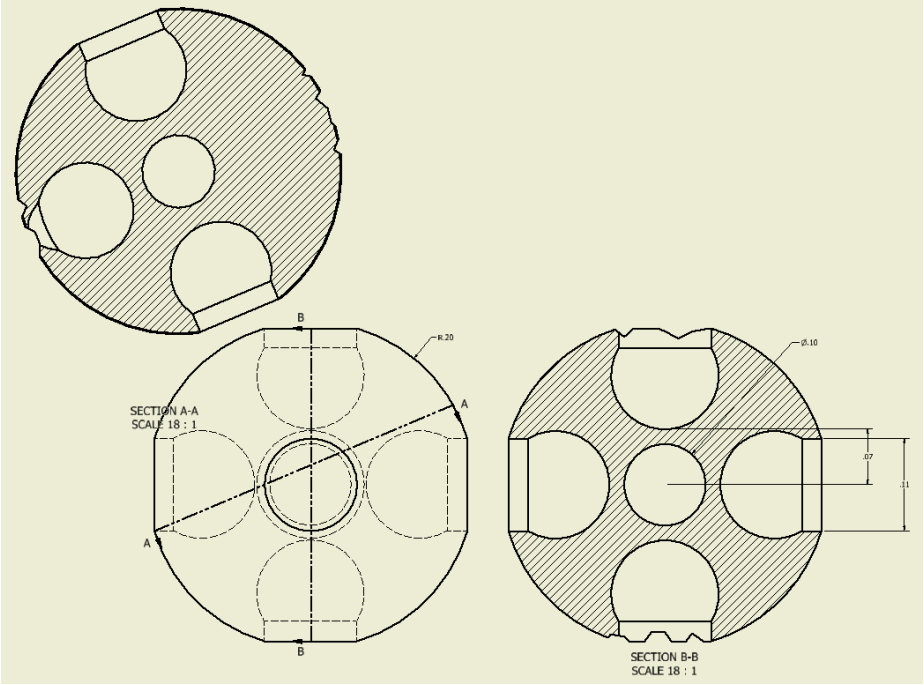

Figure 3.5: Dimensions of the model (in inches)

3.5 Procedure

For our experiments, we mounted the enclosure on the vibration shaker with the help of steel screws. We placed a thick sheet of black paper on the base of the platform to negate the effects of the steel screws on the magnets present within the units. The black background also provides a way to filter the noise while recording the video of the experiments. The shaker is connected with the power amplifier and the function generator which allows us to monitor and regulate the input frequency, amplitude and gain entered into the system. Once the system is set-up, we switch on the power supply and start the experiment. We used 12 dimer units each with two magnets arranged in a 180° angle within the unit as shown in Fig. 3.4. The units were placed in the mesh shown in Fig. 3.6 to reduce the possibility of bias. and are released into the enclosure when it is vibrating at a set frequency and amplitude. The video recording is started as the units are released into the vibrating environment, and the test matrix in Table 3.1 is filled. The units vibrate within the enclosure and when the magnetic attraction comes into play, they start forming structures.

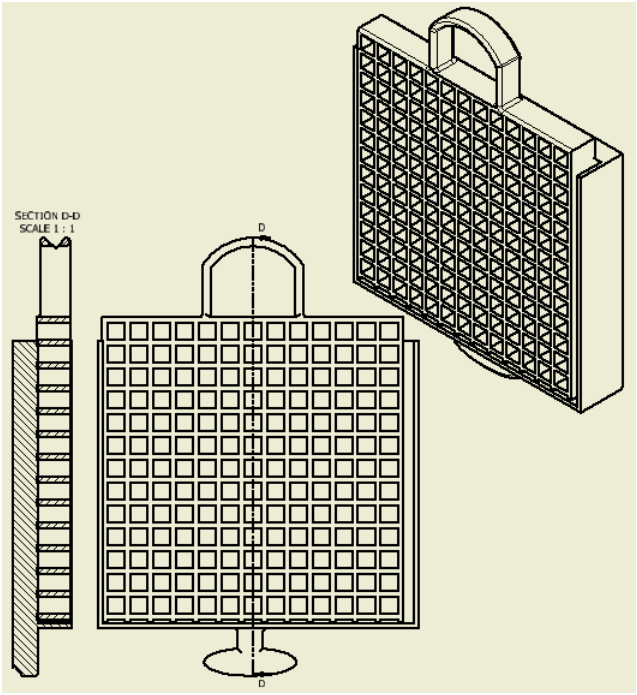

Figure 3.6: Mesh used to introduce randomness while entry of the units into the enclosure

Table 3.1: Test matrix of experiments

Frequency	Gain	Amplitude	Time to form PF structure (s)
20 Hz	Half	0.5 Vpp	24
20 Hz	Full	0.5 Vpp	12.2
40 Hz	Full	0.5 Vpp	28.79

3.6 Results: Experiments with units of 2 bonding sites

A recording of each experiment from when the units start grouping into chain formation is taken and certain number of frames are extracted from the video recording. These frames are further refined using several image processing techniques in MATLAB. We used black backgrounds while recording the experiments, to counteract the noise generated due to different colors in the extracted frames. As the units used in our experiments are spherical units, we developed a code in MATLAB to detects circles from images. The 2D Cartesian coordinates of the centers of the identified circles along with their radii, were extracted from the images with the help of this code, whose results are shown in Fig. 3.7. A total of 60 frames were selected at random from the recordings and then analyzed to extract the angles of contact between each of the units, after the structures are formed. These frames were extracted keeping in mind that the structure of the PF could be observed clearly for further analysis.

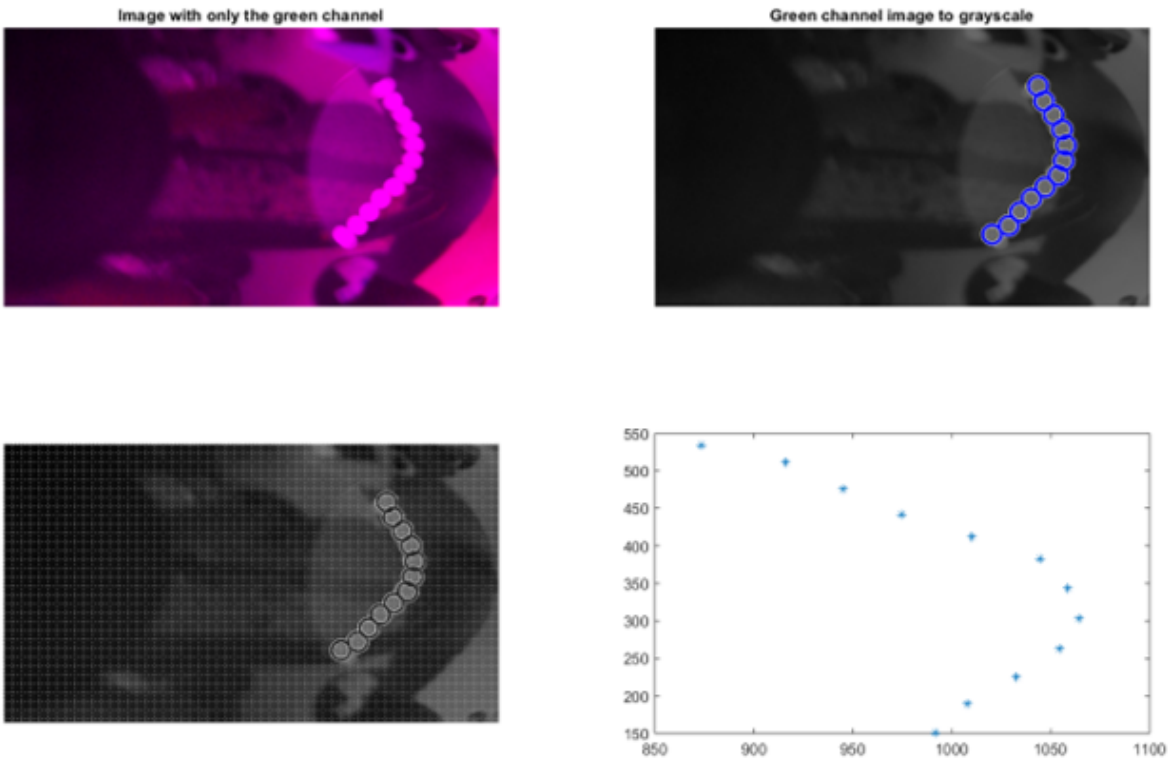

Figure 3.7: Image after applying image processing techniques in MATLAB

Calculating the angles of contact

Using the 2D Cartesian coordinates obtained from the Image processing techniques in MATLAB, we make use of the dot product for finding the cosine inverse angle using the equation

$$\vec{A}.\vec{B} = |A| \cdot |B| \cdot \cos\theta \tag{3.1}$$

$$\implies \theta = \cos^{-1} \frac{\vec{A}.\vec{B}}{|A| \cdot |B|} \tag{3.2}$$

This gives us the angle (in degrees) between the two centers of the circles, subtended at the origin which is depicted in the picture below in Fig. 3.8.

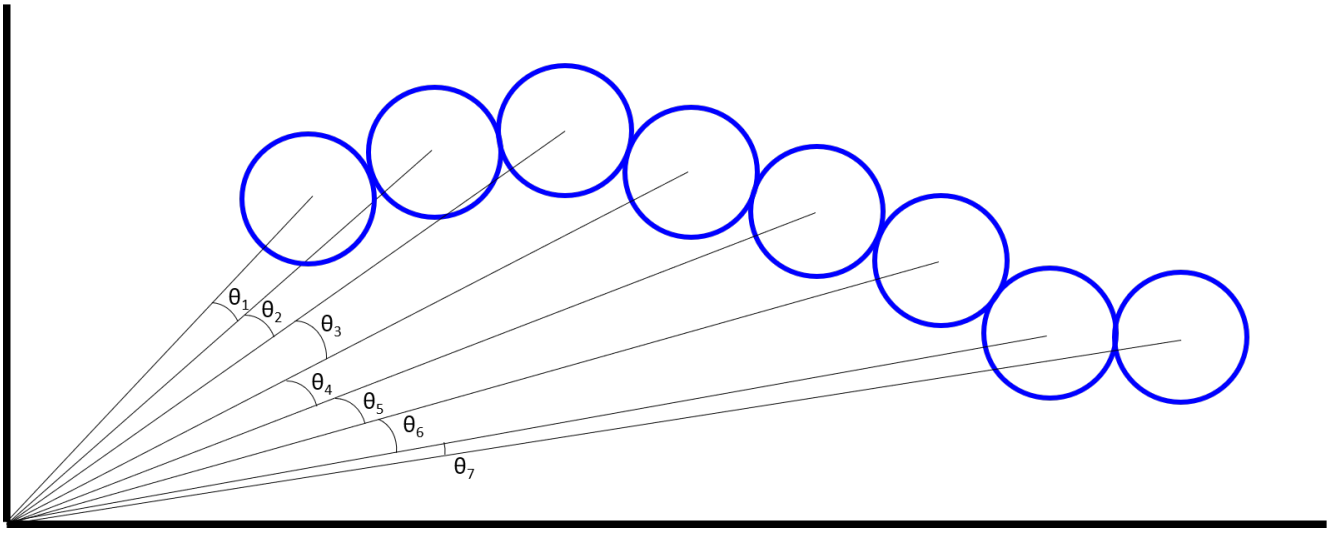

Figure 3.8: Angles subtended by the circles at the origin

Most common configurations

Once all the data of angles are collected from the above calculations, we use a grouping technique called k-means clustering to sort the data. In this method, all the observations are grouped into 'k' clusters, where each cluster is depicted by the centroid of the set of observations within that cluster. The k-means algorithm works by assuming k number of centroids at random locations in space and then arranges the input data into the relevant clusters based on distance between the individual data point and the nearest centroid of the cluster. The centroid is then reevaluated based on the mean of all the data points in that cluster. This method is continued until all the data points remain with their respective clusters. Using this approach, we grouped our data into ten clusters which are tabulated in Table 3.2.

Table 3.2: Mean angle values of the 10 clusters of angles in degrees

Cluster#	Angle 1	Angle 2	Angle 3	Angle 4	Angle 5	Angle 6	Angle 7	Angle 8	Angle 9	Angle 10	Angle 11	Freq
1	1.05	1.21	1.23	1.39	1.61	1.76	1.96	2.05	1.98	1.82	1.77	17
2	0.99	1.04	1.69	1.99	2.36	2.47	2.74	2.78	2.75	2.85	1.77	12
3	2.54	2.04	2.78	2.59	2.45	1.97	1.58	0.67	0.52	0.8	1.44	4
4	5.96	7.81	5.6	5.45	5.15	2.6	0.73	0.31	1.03	0.04	0.77	1
5	9.76	0.31	0.14	0.09	0.84	1.55	1.83	2.01	1.46	1.41	1.03	1
6	0.83	0.67	0.87	1.5	1.82	1.85	1.23	0.58	1.11	1.54	1.4	4
7	2.08	2.02	1.94	1.95	1.67	1.62	1.21	0.86	0.51	0.57	0.35	6
8	1.1	1.38	1.4	1.15	0.86	0.43	0.52	0.58	0.95	1.44	1.92	9
9	2.85	2.76	2.03	2.25	1.8	1.78	2.09	2.4	2.69	2.95	2.5	5
10	8.27	2.78	1.69	4.54	4.69	5.12	5.24	5.15	4.76	4.75	4.76	1

Based on the mean angles shown in Table 3.2, 10 different configurations of the protofilaments were developed from these clusters which are shown in the Fig. 3.9.

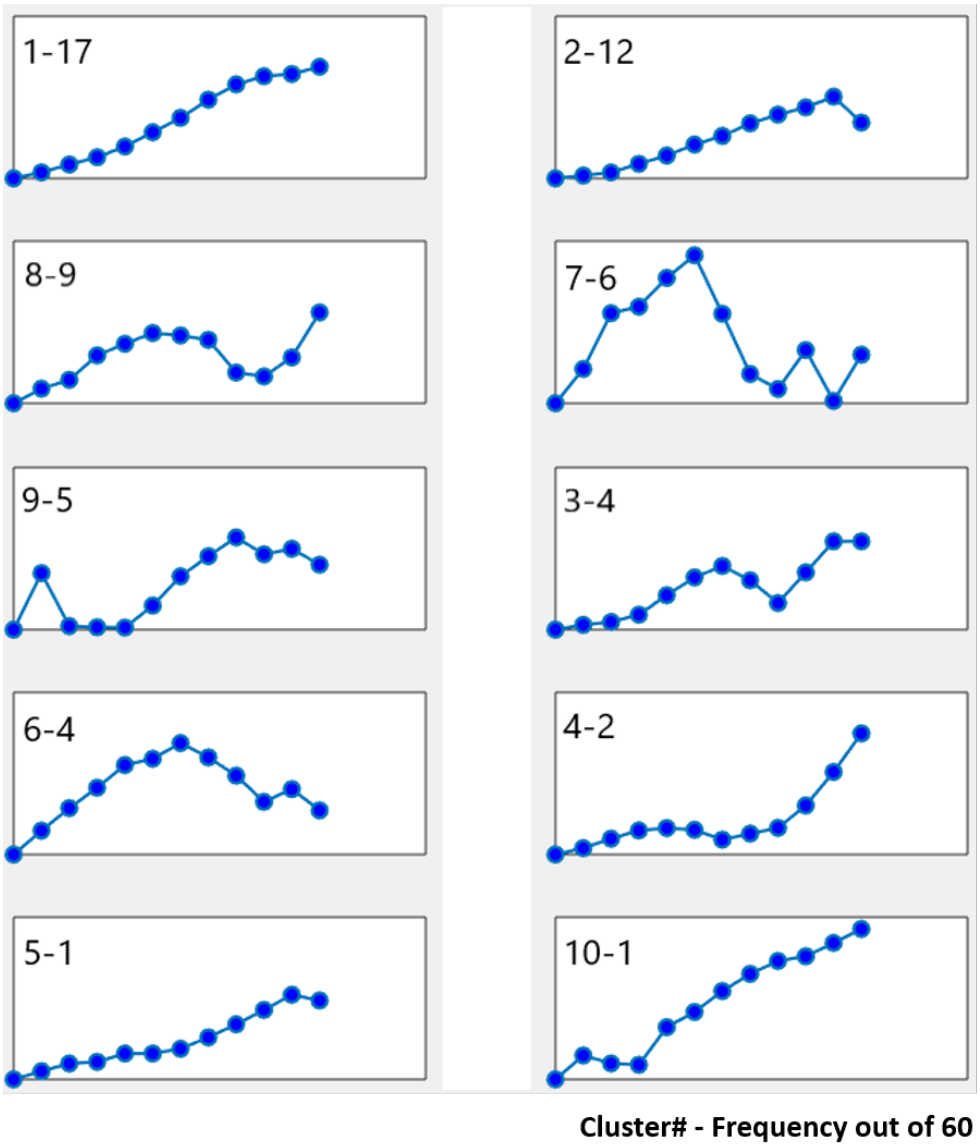

Figure 3.9: Configurations of units with 2 bonding sites

Table 3.3: X coordinates of the units for the experiments

X values	0	4.05	8.1	12.15	16.2	20.25	24.3	28.35	32.4	36.45	40.5	44.55

Table 3.4: Y coordinates of the units for the experiments

Cluster#	Y values											
1	0	0.074	0.171	0.261	0.393	0.569	0.747	0.97	1.16	1.26	1.287	1.377
2	0	0.07	0.147	0.358	0.563	0.835	1.048	1.357	1.573	1.751	2.016	1.377
8	0	0.18	0.289	0.59	0.733	0.866	0.836	0.782	0.379	0.331	0.566	1.12
7	0	0.423	1.111	1.191	1.546	1.825	1.103	0.361	0.175	0.655	0.028	0.599
9	0	0.697	0.044	0.03	0.025	0.297	0.658	0.906	1.137	0.929	0.997	0.801
3	0	0.059	0.095	0.185	0.424	0.643	0.785	0.609	0.328	0.706	1.089	1.089
6	0	0.147	0.286	0.412	0.552	0.59	0.687	0.599	0.486	0.324	0.403	0.272
4	0	0.078	0.195	0.297	0.325	0.304	0.182	0.257	0.328	0.604	1.018	1.493
5	0	0.202	0.39	0.431	0.637	0.636	0.755	1.035	1.358	1.713	2.087	1.945
10	0	0.589	0.393	0.358	1.286	1.661	2.177	2.6	2.92	3.035	3.365	3.71

To better visualize these ten different configurations obtained experimentally, we use curve fitting technique to construct a curve which could provides for a best fit to the series of data points. We used quadratic and cubic polynomials to smooth the data and improve the appearance of the plots. The curve fitting was done in MATLAB with the help of the least squares curve fit which minimizes the error between the original data and values predicted by the polynomial. The initial X and Y values from our data are shown in Tables 3.3 and 3.4, and the resulting polynomials after curve fitting are organized in Table 3.5.

Table 3.5: Curve fitting results based on X and Y coordinates

Cluster #	Best fit polynomial
1	$0.0000219x^2 + 0.0336x - 0.0752$
2	$-0.000375x^2 + 0.0621x - 0.1989$
8	$0.000077x^3 - 0.0057x^2 + 0.1273x - 0.1677$
7	$0.00016x^3 - 0.0129x^2 + 0.2689x - 0.219$
9	$-0.0000779x^3 + 0.0053x^2 - 0.071x + 0.2094$
3	$0.000023x^3 - 0.0015x^2 + 0.0493x - 0.0903$
6	$-0.00097x^2 + 0.0488x - 0.0154$
4	$0.000077x^3 - 0.0041x^2 + 0.0664x - 0.0572$
5	$0.000589x^2 + 0.02x + 0.0795$
10	$0.0000536x^2 + 0.0853x - 0.0956$

The models after curve fitting was done, are superimposed over the original experimental results and are shown in the Fig. 3.10. These polynomials provide us with a way to characterize the curves of the 10 configurations, obtained from the experiments performed on the electrodynamic shaker. This data allows us to compare the results of the curvature of these 10 configurations with the ones obtained from the simulations run in Unity 3D which will be discussed in Section 3.8.

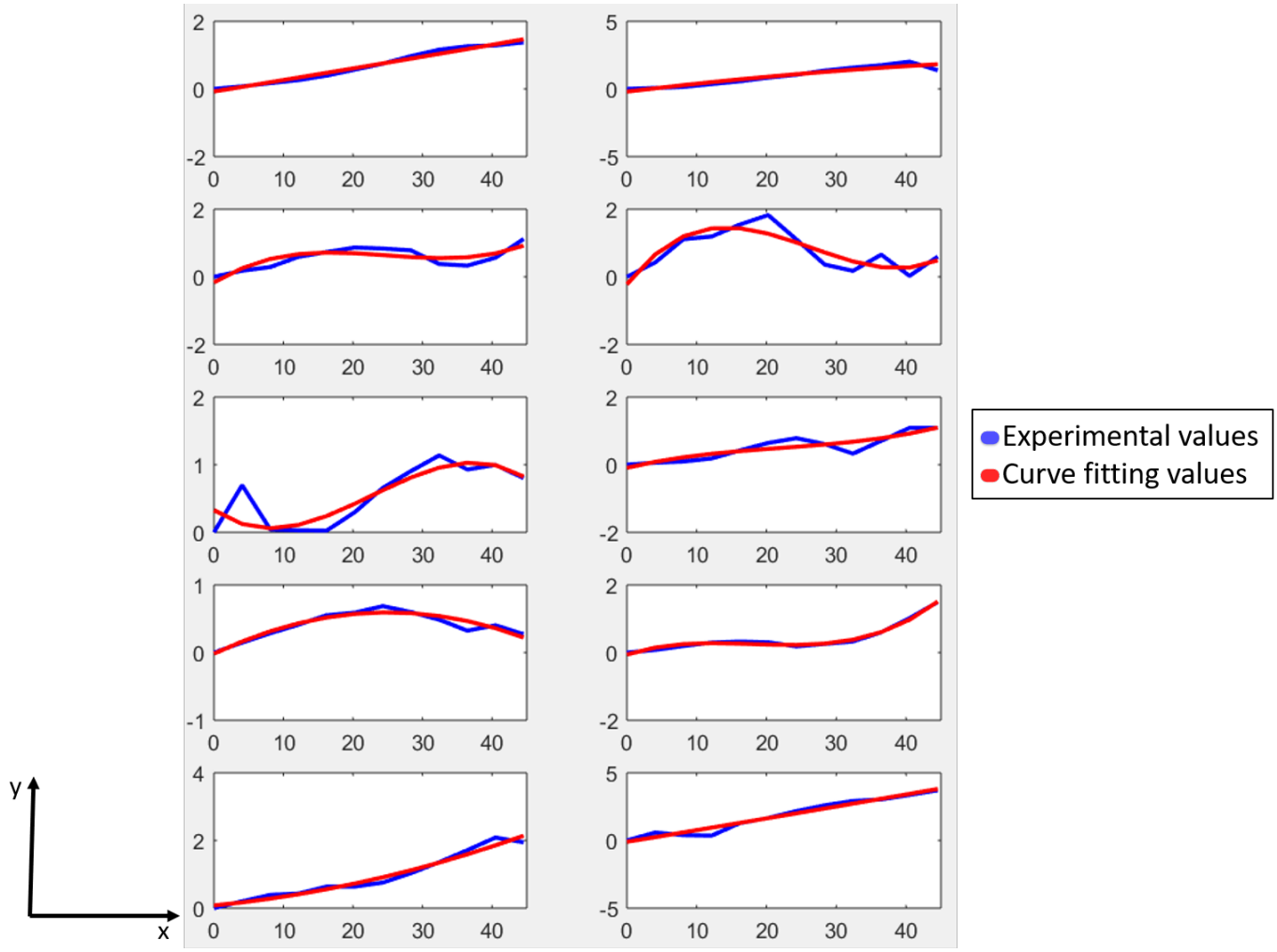

Figure 3.10: Curve fitting values superimposed on the Experimental data (original)

3.7 Results: Experiments with units of 4 bonding sites

The earlier set of experiments were conducted with 12 spherical units, each containing 2 bonding sites, i.e., two magnets per unit. These experiments demonstrated the formation of chains of units connected end to end which we refer to as protofilaments. In nature, protofilaments join laterally to form sheets which further develop a curvature, thereby forming tubes. For the next set of experiments, we used the units with four bonding sites to observe the formation of sheets like structures as in Fig. 3.11.

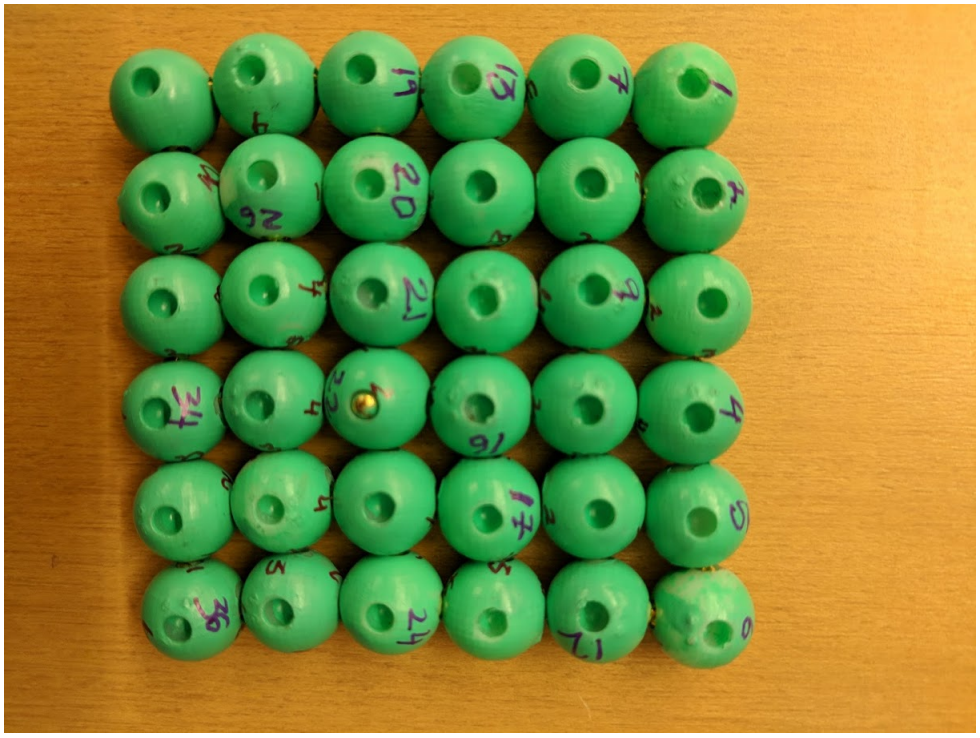

Figure 3.11: Sheet Configurations we seek to observe

With the same experimental set-up as in Fig. 3.1, we turn on the power supply and release the units into the enclosure through the mesh which introduces randomness during entry. Video recordings of the experiments were collected and the recordings were observed for common patterns. A few of the configurations observed are shown in the Fig. 3.12.

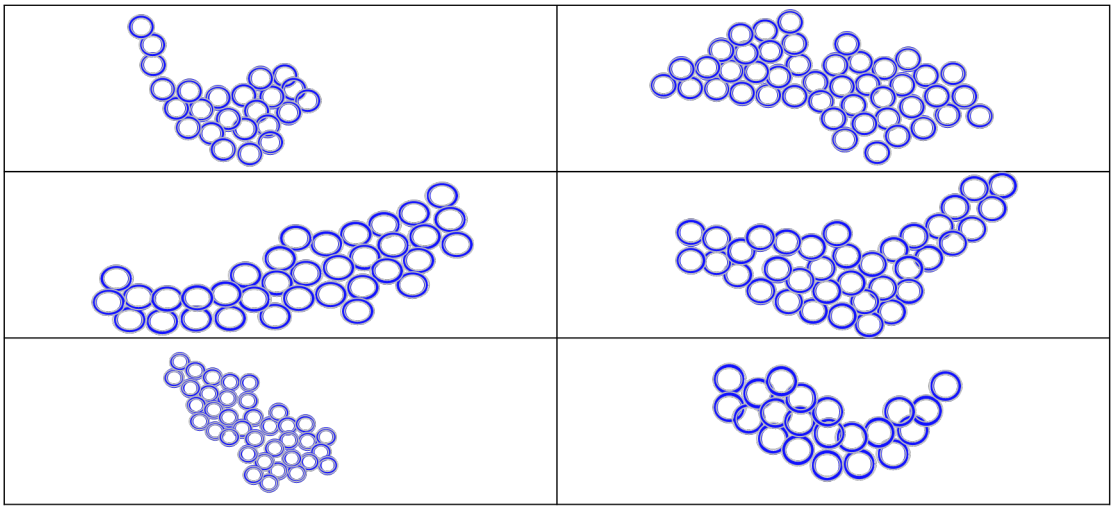

Figure 3.12: Sheet Configurations for units with four bonding sites

It can be seen from the configurations that the units do form sheets. As can be noticed from Fig. 3.13(b), the units try to join at their ends to form a tube. But due to factors like the weight of the units and gravitational forces, it has been observed that the single layered sheet breaks into two and collapses on one another, thereby forming aggregates.

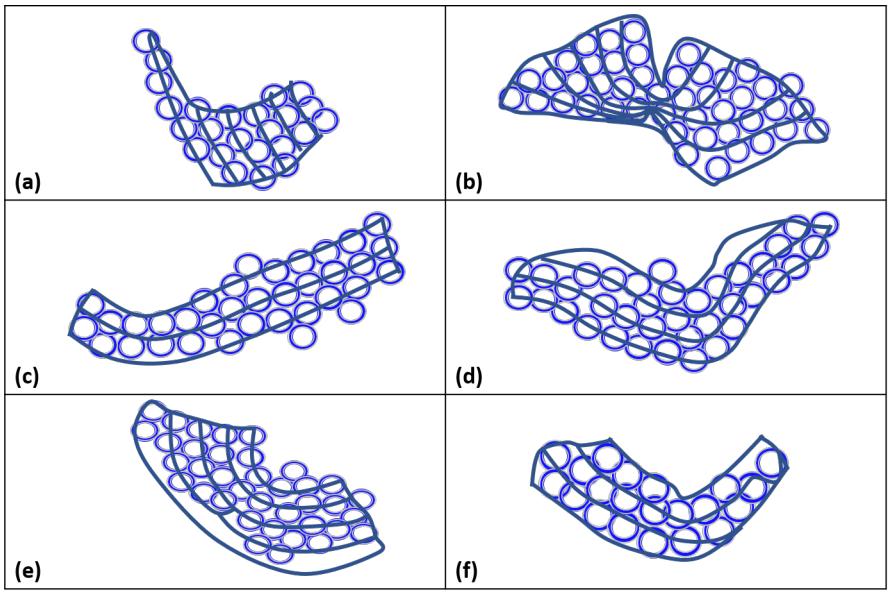

Figure 3.13: Sheet Configurations for units with 4 bonding sites

As we couldn't counteract for gravity at that time, we focused on the results with units with two bonding sites which connect together to form protofilaments.

3.8 Simulations in Unity 3D

Unity is a cross-platform game engine which has an built-in physics engine which enables users to run 2D and 3D, highly realistic and high-performance simulations on a computer. It provides a platform for recreating a real system in a virtual environment and hence, was chosen to execute our simulations on. The experiments performed for studying self assembly in microtubules involved many logistics, like 3D printing the tubulin units, purchasing spherical magnets, designing and 3D printing the enclosure, setting up the electrodynamic shaker, etc. Simulations in Unity provide for a simpler way to recreate the results of our experiments with better accuracy and little possibility of error, cutting down setup time and cost. As the

simulations are a more effective way to obtain results when compared to the experiments, we seek to obtain a correlation between these two methods in this study.

Aggarwal et al. employed molecular dynamics simulations to study the assembly process using wedge shaped monomers which are capable of bonding laterally and vertically to develop artificial microtubules. Their results explain the optimal range of interaction strengths to realize artificial tubule formation. It was observed that tubules bind on collision, thereby breaking and forming new bonds [31].

Spoerke et al. utilized molecular simulations to understand intermolecular interaction strengths and changes in molecular shape which controls assembly in microtubules. They modeled α/β-tubulins as tubule-forming wedge-dimers and also employed a compacted angle of 15° to resemble bent tubulin [32].

Zakharov et al. employed simulations using a coarse grained Brownian dynamics approach where monomers interact with their neighboring subunits at four contact points and catastrophes in the microtubule arise owing to the fluctuations in the number of protofilament curls [33].

Parameters

The version of Unity used for the simulations is Unity 2018.2.10 and was run on a Windows 10 PC with a configuration of 4.01GHz Clock Speed (i7-6700K), 64 GB RAM, NVIDIA Quadro K2200 GPU and high speed solid-state drive.

As we were trying to recreate the same environment conditions as that of the experiments, the entire population of the units considered is 12. Each of these units, as can be seen in Fig. 3.14, is spherical and represent a single tubulin protein. We have used the spherical shape to promote formation of the protofilament structure. They have two bonding sites, set at 180° apart from each other so as to enable lateral bonding to enable the formation of chain-like protofilaments, as found in the experimental results.

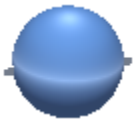

Figure 3.14: Tubulin unit, with cube shaped bonding sites set laterally at 180° apart

The red base shown in Fig. 3.15 acts as the vibrating platform for the simulations and measures 1.8×20 $(d \times h)$ units. The units measure $2 \times 2 \times 2$ $(l \times b \times h)$ units, while the cubic bonds are set at $0.3 \times 0.3 \times 0.3$ $(l \times b \times h)$ units.

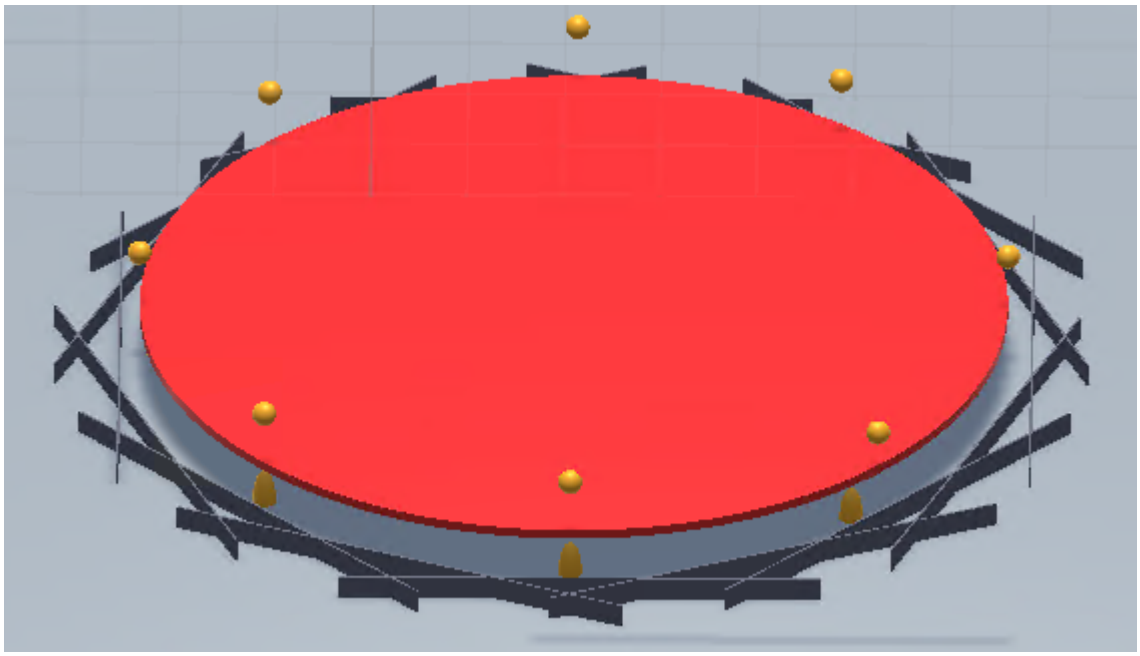

Figure 3.15: Platform for simulations

Functionality of the simulator

The simulations were run in Unity 3D, using a custom made program in C#, developed by Sarma OVS, et al in the DICE lab at UGA College of Engineering for studying the self organization in microtubules, as an extension of his Master's level thesis [34]. The simulation set-up is shown in Fig. 3.16. The platform is excited by the physics engine based on the frequency and displacement amplitude parameters. There are spring joints applied to the platform to keep it in place and a random force is applied to impart vibratory motion into

the platform. Each of the spherical units have two cubes laterally arranged on either side 180° apart, which mimic the magnets used in the experiments.

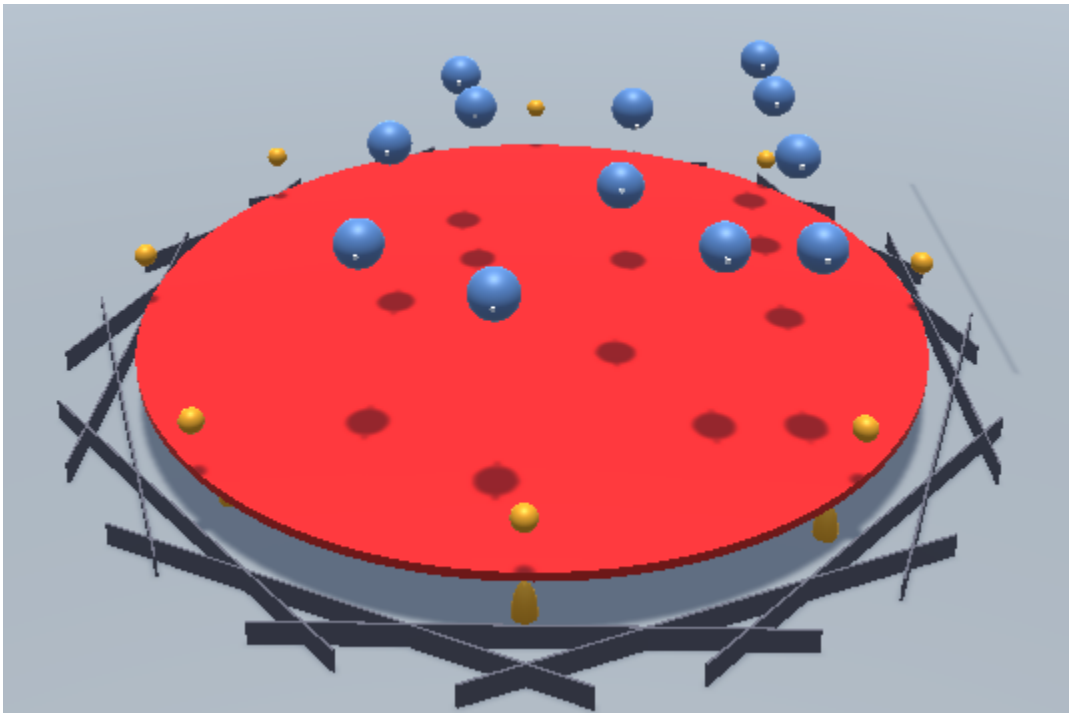

Figure 3.16: Platform for simulations

The simulation starts when the 12 spherical units are dropped into the enclosure, from a fixed height of 20 units. When the base starts vibrating, the units inside are taken into an excited state. Due to the interaction of the cubical bonds when they are in close proximity with bonds of neighboring spherical units, the formation of chain like protofilaments are observed. Once there is a bond association between two units, the bond flag turns true, and the bond becomes inactive, i.e does not accept linkage with any other units through that bond. Once all the units are linked with one another, we capture images of their structures to analyze the angle of contact subtended by the units with one another.

3.9 Results: Simulations in Unity

Once the images are extracted from the recorded videos, they are processed in MATLAB using image processing techniques to find circles. An algorithm based on Circular Hough

Transform (CHT) is used for identifying circles in the images because of its robustness in presence of noise and shifting illumination. The X, Y Cartesian coordinates of the centers of the identified circles, along with their radii are obtained from this algorithm. We then calculate the angles of contact using Eq. 3.2 and apply the k-means clustering technique which is explained in detail in Section 3.6, to obtain the most commonly observed structural configurations. The mean angle values of the ten most commonly observed configurations are listed in Table 3.6. The Y values are calculated from the X values in Table 3.3 and angles from Table 3.6, using the tangent function and are tabulated in Table 3.7. Similar to the experimental results, curve fitting polynomials are matched to the results obtained from Unity and are shown in Fig. 3.18. These values are then compared with those calculated from the experimental results to look for similarities. As can be seen in Fig. 3.19, both the simulation and experimental values have similar curvatures for the ten protofilament configurations.

Configurations obtained from our experiments and simulations are comparable with the results of Pearce et al. where they observed the shape evolution of microtubules by computational methods [35]. Vandelinder et al. utilized biomolecular motors to develop nano-fluidic transporters and observed self assembly, where they observed different curved microtubule configurations which help to strengthen our protofilament configurations obtained [36]. Below are some images obtained from the experiments and simulations:

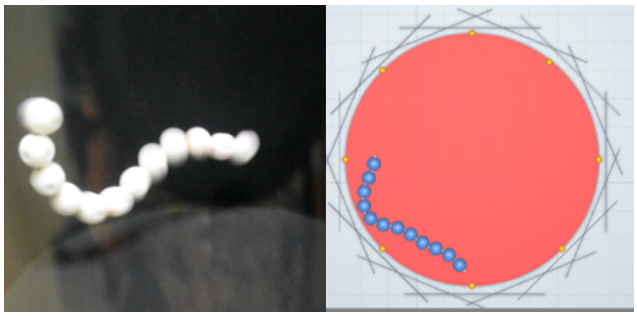

Figure 3.17: Left: Image from experimental methods; Right: Image from simulation methods

Table 3.6: Mean angle values of the ten clusters of angles in degrees, from simulations

Cluster#	Angle 1	Angle 2	Angle 3	Angle 4	Angle 5	Angle 6	Angle 7	Angle 8	Angle 9	Angle 10	Angle 11	Freq
1	0.91	1.52	1.86	1.6	0.75	0.49	1.3	1.76	1.68	1	0.62	4
2	2.29	1.58	0.92	0.95	1.22	1.11	0.06	1.01	1.05	1.15	1.26	2
3	2.28	2.2	1.75	1.31	0.63	0.59	1.45	1.89	1.88	1.71	1.62	5
4	0.68	0.8	0.73	0.56	0.58	0.52	0.59	0.81	0.97	1.23	1.26	18
5	1.35	1.21	0.65	0.82	1.7	2.01	1.74	1.11	0.45	0.59	0.79	4
6	1.57	1.07	0.55	0.29	0.48	0.91	1.5	1.83	1.83	1.69	1.51	11
7	0.36	0.95	1.69	2.01	1.56	0.9	0.59	0.77	1.44	1.75	1.6	5
8	2.28	2.33	1.66	0.66	0.41	1.06	1.42	0.9	0.64	1.07	1.39	6
9	2.33	1.86	1.95	2.34	2.35	1.61	0.79	1.17	1.33	1.54	1.42	2
10	2.47	1.77	0.85	0.35	1.5	1.86	0.99	0.78	1.19	1.11	1.28	3

Table 3.7: Y coordinates of the units for the simulations

Cluster#	Y values											
4	0	0.0481	0.1131	0.1548	0.1583	0.2050	0.2205	0.2919	0.4581	0.6171	0.8696	0.9799
6	0	0.1110	0.1513	0.1166	0.082	0.1696	0.386	0.7424	1.0352	1.1646	1.1949	1.1744
8	0	0.1612	0.3296	0.3521	0.1866	0.1449	0.4496	0.7028	0.5090	0.4072	0.7564	1.0810
3	0	0.1612	0.3112	0.3712	0.3705	0.2227	0.2502	0.7176	1.0692	1.1964	1.2091	1.2600
7	0	0.0254	0.1343	0.3585	0.5685	0.5515	0.3817	0.2919	0.4355	0.9163	1.2374	1.2444
1	0	0.0643	0.2149	0.3946	0.4525	0.2651	0.2078	0.6434	0.9956	1.0691	0.7069	0.4821
5	0	0.0954	0.1711	0.1378	0.2319	0.6010	0.8528	0.8612	0.6278	0.2863	0.4171	0.6143
10	0	0.1747	0.2503	0.1803	0.99	0.5303	0.7891	0.4899	0.4411	0.7572	0.7847	0.9954
2	0	0.162	0.2234	0.1951	0.2686	0.4312	0.4708	0.0297	0.5712	0.6681	0.8130	0.9799
9	0	0.1648	0.263	0.4137	0.662	0.831	0.683	0.3909	0.6617	0.8463	1.0888	1.1043

Table 3.8: Curve fitting results based on X and Y coordinates after simulations

Cluster #	Best fit polynomial
1	$0.000597x^2 - 0.0062x + 0.068$
2	$0.000543x^2 + 0.0074x - 0.0.0122$
8	$0.000334x^2 + 0.0028x + 0.1309$
7	$0.000495x^2 + 0.0073x + 0.0892$
9	$0.000456x^2 + 0.0051x + 0.0828$
3	$-0.000378x^2 + 0.0346x - 0.0512$
6	$-0.000738x^2 + 0.0459x - 0.1028$
4	$0.0000908x^2 + 0.01556x + 0.0482$
5	$0.000395x^2 + 0.000502x + 0.1169$
10	$-0.000131x^2 + 0.0273x + 0.076$

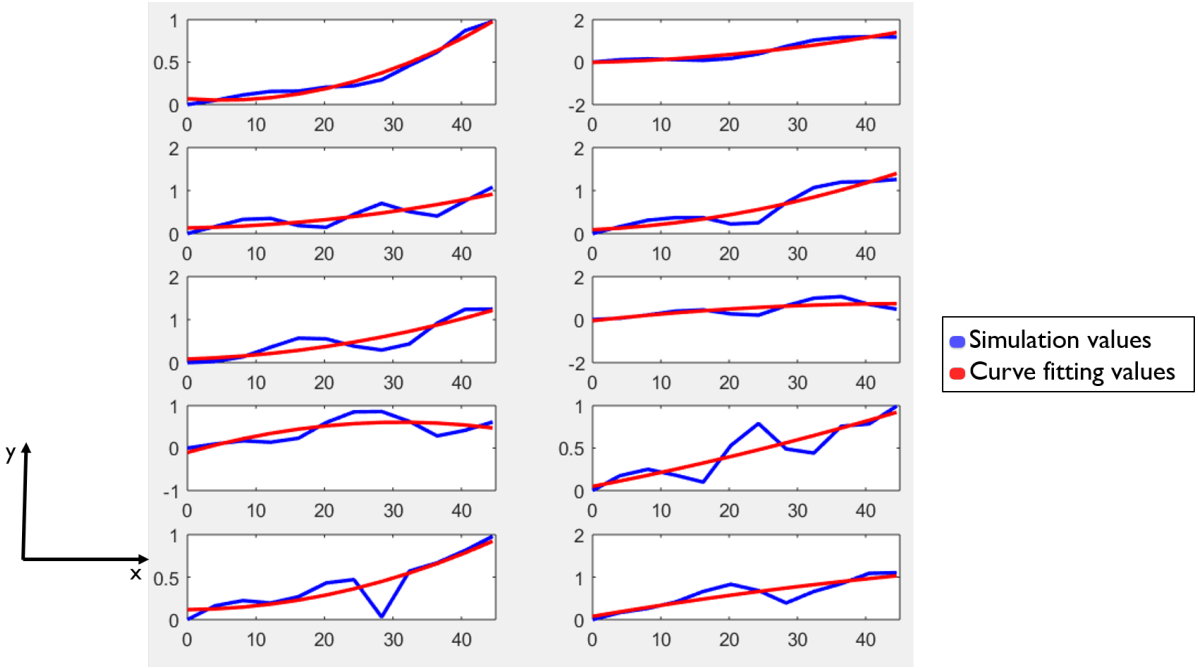

Figure 3.18: Simulation results superimposed with curve fitting polynomials

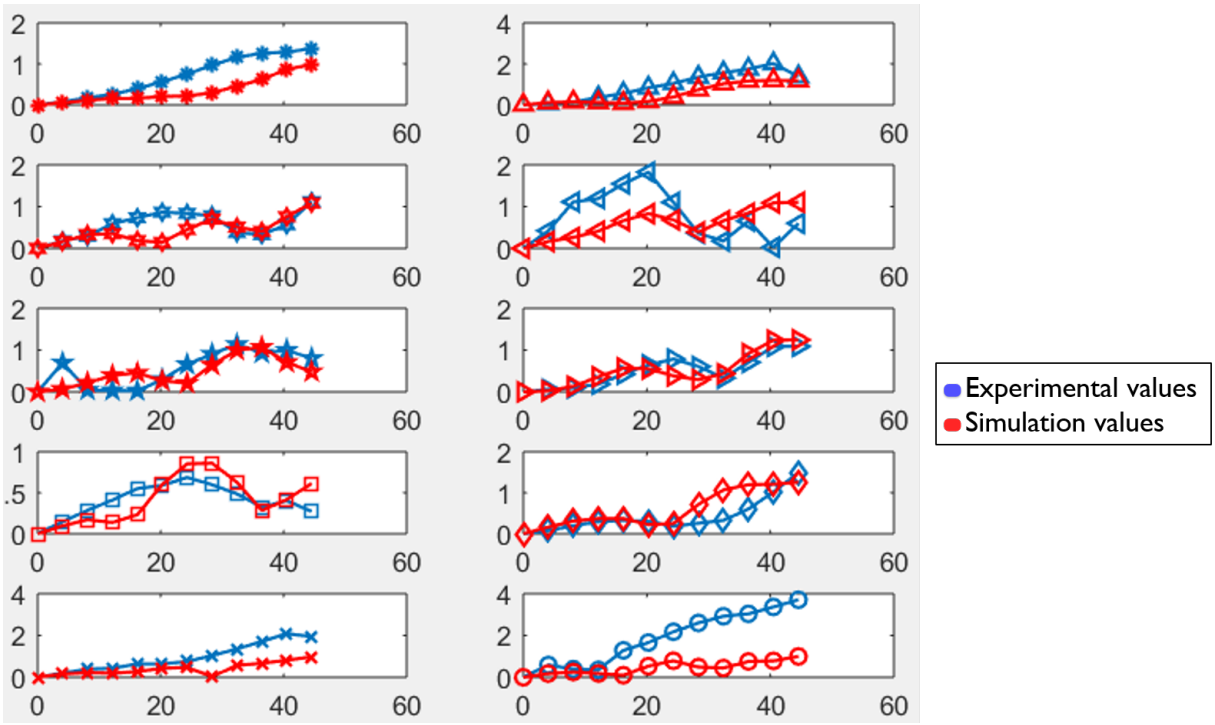

Figure 3.19: Results: Experiments vs simulations

Chapter 4

Structural Analysis of a Protofilament using FEA

In Chapter 2, it has been mentioned that microtubules play a critical role in maintaining the structural framework of a cell, and hence, we analyze the strength of these structures as a way to learn about them. Tubulin dimers can be considered as the fundamental units of a microtubule; and as the dimers bind together due to the synergy of tubulin with different MAPs, along with the chemical interactions with GTP and GDP, protofilaments are formed. The bonding between these dimers within the protofilament are considerably stronger than the bonds between protofilaments laterally [23]. Hence, we modeled the structure of a typical protofilament to study how it responds to different kinds of loads in a finite element analysis method.

Janosi et al observed from their study of microtubules with electron micrographs, that they were made of 10 to 16 protofilaments, with either 13 or 14 protofilaments in 90% of the cases in their study. They have made observations that the change in the lateral bond strength between protofilaments plays a role in the polymerizing and deploymerizing of the MTs and also, that tere is a particular correlation between protofilament number and curvature at the MT tips [37].

Zhang et al used a structural mechanics model of a microtubule to observe the configuration effect on the Young's modulus, Shear modulus, bending stiffness and persistence length of the microtubules. They also noticed from their experiments that the protofilament number within a microtubule ranges from 12 to 15 and that the Young's modulus is fairly independent of the different microtubule configurations and stays at a constant value of 0.83 GPa [38].

Shahinnejad et al. developed a 3D finite element model and investigated the mechanical properties of axonal microtubule bundles by studying the strain-stiffening behavior of these bundles under uniaxial tension and torsional loading [39].

4.1 3D MODELING OF THE PROTOFILAMENT GEOMETRIC STRUCTURE

Considering the different vital microtubule functions happening in a cell, there has been a lot of recent studies targeted at investigating the mechanical properties of the microtubule. However, there has been a dearth of quantitative information of the microtubules at the molecular level. The aim of this study is to analyze the stresses and the effect of the protofilament curvature by means of a static structural analysis using finite element methodology. We attempt to focus on the mechanical behavior of the protofilaments as a means to understand the microtubules at a more basic level.

The basic unit of a microtubule is the tubulin dimer which bonds longitudinally to other dimers thereby forming protofilaments. We assume the tubulin monomer to be spherical in shape for developing our 3D model [30]. Chrétien et al. observed that the number of protofilaments varied from twelve to seventeen, with sixteen and seventeen protofilaments being in the minority and thirteen being the majority population [10]. Our protofilament model consists of 12 tubulin units modeled as spheres of diameter $4.05\mu m$ and fixed at one end, while free at the other end.

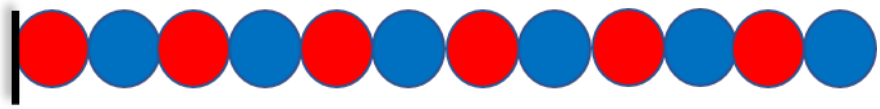

Figure 4.1: Protofilament

The response of this protofilament model to different loading cases has been studied by using a finite element analysis approach. The basic steps involved in FEA is the modeling of the components, assignment of the material properties, solving the equations and post processing of the results. Modeling of the components is achieved by drawing it in a CAD or

a solid modeler package, which could later be imported into a FEM software. We used ANSYS Workbench for our FEA simulations, which is a global leader in engineering simulations which is widely used to predict how product designs behave in real-time scenarios. Once the 3D geometry is created, the material properties are entered into the FEM system to apply to the component. Meshing of the component, which is the core of the FEA method is performed next and boundary conditions are applied following which the system is solved according to the constitutive equation as per the problem description.

4.2 Physical - Mechanical properties of the protofilament system

Material properties which were observed with previously conducted experimental and computational studies around the world have been summarized in Table 4.1.

Table 4.1: List of different properties of microtubules based on prior studies

Property	Value	Method
Young's modulus	1.2GPa	[40]
Young's modulus	1.85 GPa	[41]
Young's modulus	1.5 GPa	[42],[43]
Young's modulus	0.8 - 0.85 GPa	[38]
Young's modulus	0.5 - 2 GPa	[44], [24]
Shear modulus	1.4 MPa	[23]
Shear modulus	0.163 - 6.421 MPa	[45]
Density	1470 kg/m^3	[46]
Length	$1 \sim 8$ μm	[46]
Poisson's ratio	0.3 kg/m^3	[46]

Material properties

The α and β tubulin dimers are protein elements which we modeled as an isotropic elastic material with the material properties as shown in Table 4.2.

Table 4.2: Material properties used for our model

Property	Value
Density	1470 kg/m^3
Young's modulus	1.85 GPa
Poisson's ratio	0.3
Tubulin diameter	4.05 μm
Beam (circular c/s) diameter	0.2025 μm

Geometry

The geometry for our system was modeled directly in the ANSYS DesignModeler software in which 2D geometry can be created, edited and converted to 2D or 3D models. The protofilament is fixed at the left end and is free at the right end. Each of the spheres in Fig. 4.2, represents a tubulin unit, and are bonded to each other which does not allow for any sliding or separation between edges of the spheres. Each tubulin sphere measures 4.05 μm and the entire protofilament measures upto 48.6 μm with a volume of 417.42 μm^3.

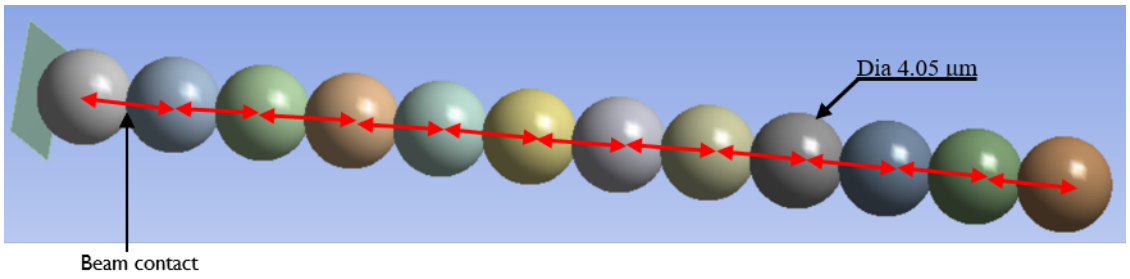

Figure 4.2: Protofilament model designed in ANSYS DesignModeler

The tubulins are connected to each other by means of a beam of circular cross-section of radius 0.2025 μm. The beam material is the same as that of the tubulin material.

Mesh

We used the proximity and curvature size function to generate the mesh for the model, with a minimum element size of 0.4 μm. The smaller the element size for the mesh, the higher is the accuracy of the results. This has been observed by conducting a mesh convergence study: first for a cantilever beam, and then for the straight protofilament model, applying

the material properties as in Table 4.2. Mesh convergence determines the number of elements required for the model to produce analysis results, which do not vary much by changing in the mesh size.

Mesh convergence study of cantilever beam

For this study, we considered the BEAM188 element which has at least six degrees of freedom at each node, including translations in x, y and z directions and rotations about x, y and z directions citeansys. As this element is based on Timoshenko beam theory, it is well-suited for linear, large rotation and large strain nonlinear applications, and hence, we chose this element for solving our FEM problem. We first modeled a beam of rectangular cross-section (seen in Fig. 4.3) in ANSYS DesignModeler, assigned the material properties, generated a mesh containing 25 elements and applied a bending force of 10N on one end while keeping the other end fixed. Deflection results obtained from these computations were then compared with similar simulations conducted in ANSYS APDL using BEAM188 specifically. The results (seen in Fig. 4.4) were shown to be identical, which meant that we could proceed to solve our models in ANSYS Mechanical for further simulations as it has a better user interface.

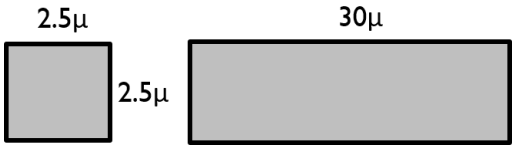

Figure 4.3: Model dimensions for convergence study

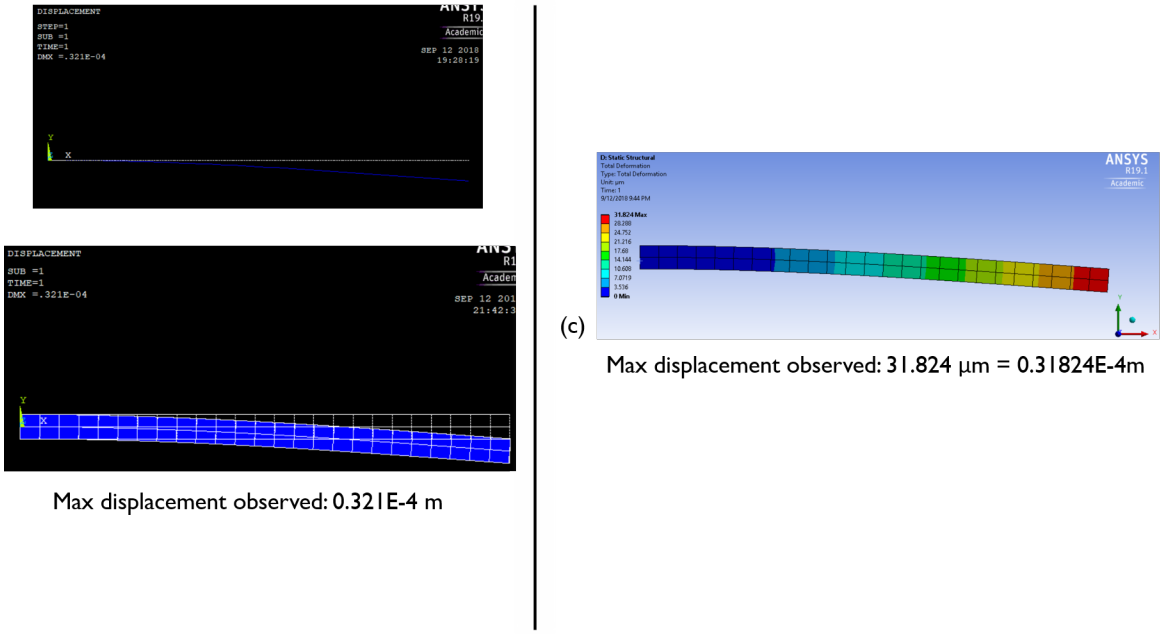

Figure 4.4: Response to bending in APDL: (a) Line view of the cantilever (b) 2D view of the cantilever; (c) Response to bending in ANSYS Mechanical

Now, we consider varying number of elements to check for mesh convergence. The number of elements in the mesh and the deformation values when the model is subjected to a bending force of 10N are tabulated in Table 4.3. Based on the values in the below table, we plotted the number of elements vs the bending deflection values to obtain a convergence chart as shown in Fig.4.5. It can be seen from the convergence chart that the deflection values get saturated without much fluctuations, as the mesh is made finer by increasing the number of elements in the mesh. Thus, we can conclude that the smaller the element size, the accurate the results are. Another key point to note is that as the mesh size is made finer, the computational time also increases along with the accuracy which is a major deciding factor in choosing the mesh size for our computations.

Table 4.3: Inputs to check for Mesh Convergence

No. of elements	Deformation (μm)	% change in elements	% change in deformation
225	148790	12	0.013442
252	148810	7.14	0.01344
270	148830	13.33	0.013438
306	148850	98.69	0.06718
608	148950	13.16	0.0067
688	148960	81.69	0.0403
1250	149020	20	0.0067
1500	149030	145	0.0403
3675	149090	120.41	0.0201
8100	149120	212.96	0.0268
25350	149160	639.65	0.0201
187500	149190	-	-

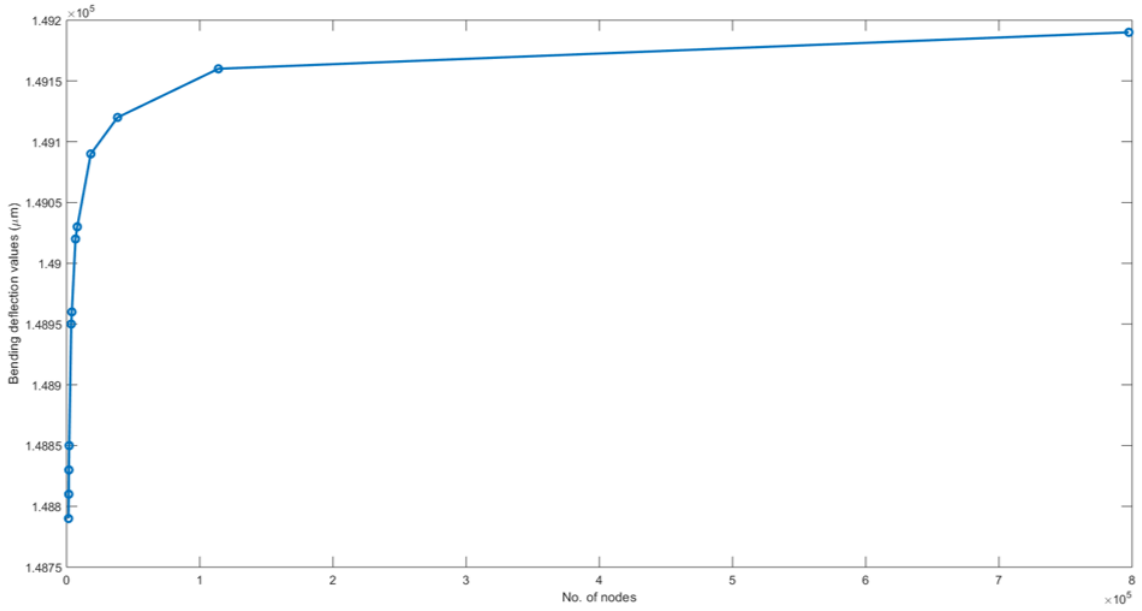

Figure 4.5: Convergence study chart for cantilever beam

The bending deflection results obtained from the analytical solution ($\delta = PL^3/(3EI)$) as 0.1494 m closely matches to the 0.14912 m obtained from our results. The deformation due to tension calculated analytically ($PL/(AE)$) is 25.946 μm, and is in alignment with the 25.839 μm obtained from our simulations. This shows that our approach is in line with the analytical solutions.

Mesh convergence study of straight protofilament

After the successful checking of convergence study for the cantilever beam, we extend the same approach towards the straight protofilament model shown in Fig. 4.2. As seen in the convergence study for cantilever beam, we can see that the change in deformation values starts to settle down as the number of elements in the mesh are increased. The minimum element size corresponding to the maximum number of elements shown in Table 4.4, is 0.3 μm

Table 4.4: Inputs to check for Mesh Convergence for straight PF model

No. of elements	2527	2551	3164	4981	6631	10107	16050	29212	56198
Deformation (μm)	0.058158	0.069269	-0.04882	0.01279	0.08344	-0.28884	0.040087	-0.02297	0.025587

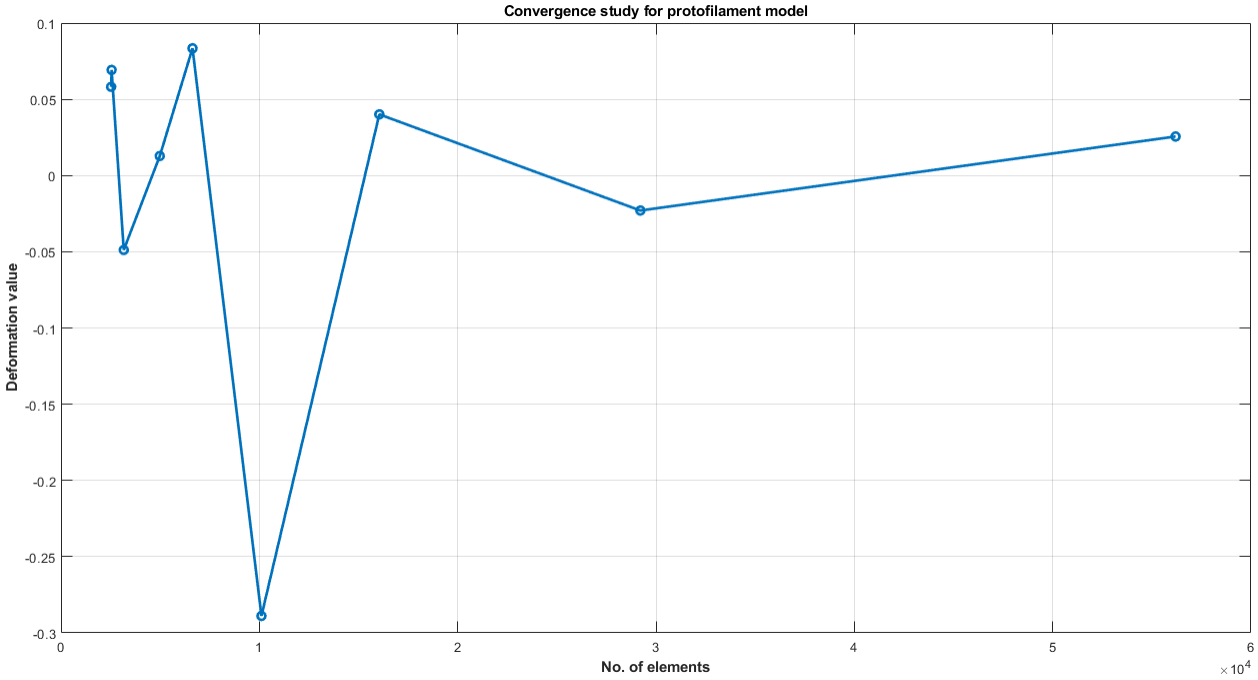

Figure 4.6: Convergence study chart for straight protofilament model at the right end

Loading conditions

We applied three major types of loadings for our simulations:

1. Tension: A tensile force varying between 0.01 μN and 15 μN was applied in multiple computations as shown in the figure below:

Figure 4.7: Tension applied on protofilament model

2. Bending: A bending force varying between 0.01 μN and 10 μN was applied in multiple computations as shown in the figure below:

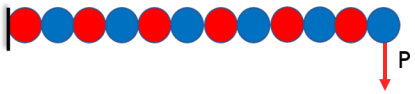

Figure 4.8: Bending force applied on protofilament model

3. Torsion: A torsional moment varying between 0.01 $\mu N.\mu m$ and 20 $\mu N.\mu m$ was applied in multiple computations as shown in the figure below:

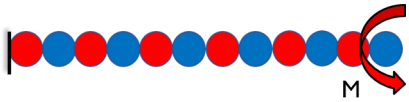

Figure 4.9: Torsional moment applied on protofilament model

Protofilament configurations

The geometry considered for our simulations until now is a straight protofilament where the tubulin dimers are joined end to end at 180° angle between each of them. The angles of contact obtained from our experiments from Table 3.2 are used here to construct ten different protofilament configurations. These different PF configurations are now subjected to the same boundary conditions discussed in Section 4.2, and studied to observe the variation of the stresses relative to the protofilament curvature.

4.3 Finite element analysis of protofilament structure

In this section, we present a FEM model to study the mechanical behavior of the microtubules under different loading conditions. Analysis involved the application of a uniform force or moment on the free end of the protofilament model as illustrated in figures 4.7-4.9. A computer with Windows 10 operating system, Intel Core i7-6700K CPU @ 4.00 GHz and 64 GB RAM was used to carry out a static structural analysis in ANSYS ® software version 19 (ANSYS Inc., Canonsburg, PA, USA). The mean angles of contact determined in Table

3.5 are used to calculate the orientations and positions of the tubulin in each of the protofilament configuration. The eleven protofilament configurations under study are demonstrated in Fig. 4.10.

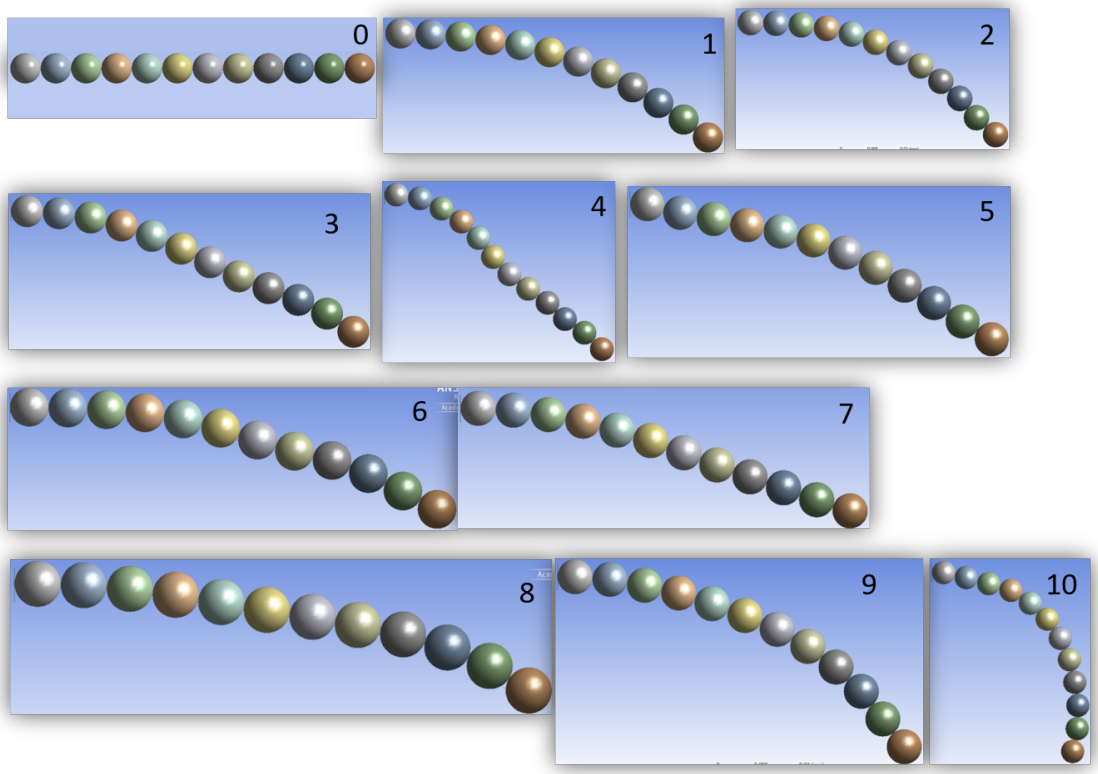

Figure 4.10: The eleven protofilament configurations obtained from Experimental results discussed in Section 3.6

4.4 Results: Structural analysis of protofilaments

It is understood from Table 4.5 that the protofilament configurations 2, 4, 9 and 10 have the higher curvatures and configurations 0, 6, 7 and 8 have the least varying curvatures.

Table 4.5: Curvatures of all the PF configurations under study

PF #	Radius of curvature (μm)	θ	Curvature (K)
1	398.1916	0.1119	0.0025
2	23.2494	-1.9171	-0.043
8	15.6004	-2.8566	-0.0641
7	3.9274	-11.3444	-0.2546
9	92.1154	0.4837	0.0109
3	235.474	0.1892	0.0042
6	9.0355	-4.9306	-0.1107
4	8.2872	5.3788	0.1207
5	148.228	0.3008	0.0067
10	162.1201	0.2757	0.0062

Figures 4.11, 4.12 and 4.13 show the deformation of the protofilaments relative to the tension, bending and torsion respectively. It can be seen in Fig. 4.14 (a) that the deformation due to tension for the: configuration 0 which is a straight PF, is the least; and that for configuration 4 which is the highest curved PF models, is the highest. It can be inferred from Fig. 4.11, that the deformation of the model due to tension increases on increase in the

curvature of the PF. There is an inverse relation between the slope of the curves and the rate of change in the deformation, which means that as the slope of the PF configuration decreases, the deformation due to tension also increases non-linearly at a slightly higher rate.

From the bending - deflection graph in Fig. 4.12, we can see that the deformation is lowest for the PF having highest curvature, and the deformation keeps increasing with decrease in curvature. The plot clearly shows that the minimum deformation is observed for PF # 10 and is highest for PF# 8 which can be observed in Fig. 4.12 as well. It is also observed that when there is a very low force applied on the PF, there is a proportional small change in length of the PF. In other words, as the magnitude of force applied increases, the deformation increases proportionately, which can be seen in the plot where, when a bending force of 0.01 μN is applied, all the eleven protofilament models do not show much increase in deformation. Closer inspection of this plot shows that there is not a significant change in deformation at low loads, which could mean that curvature of the protofilament does not make a significant impact at lower bending loads.

The torsion-deflection curve shown in the Fig. 4.13, indicates that the deflection is the lowest for the PF#0, which has the lowest curvature. It is also seen that the rate of change of length of the protofilament increases with the decrease in the slope of the curves. The highest deformation occurs to PF#10, which has one of the higher curvatures among the eleven PF models. Also, the curvature does not have a noticeable effect on the deformation at low torsional moments.

The distribution plot in Fig. 4.14 illustrates that the deformation is the least at the left end and is the maximum at the right end, which shows an increasing trend in the deformation due to different loading conditions which makes sense, as the left end is fixed. These results are in line with Jong Won et al. [47].

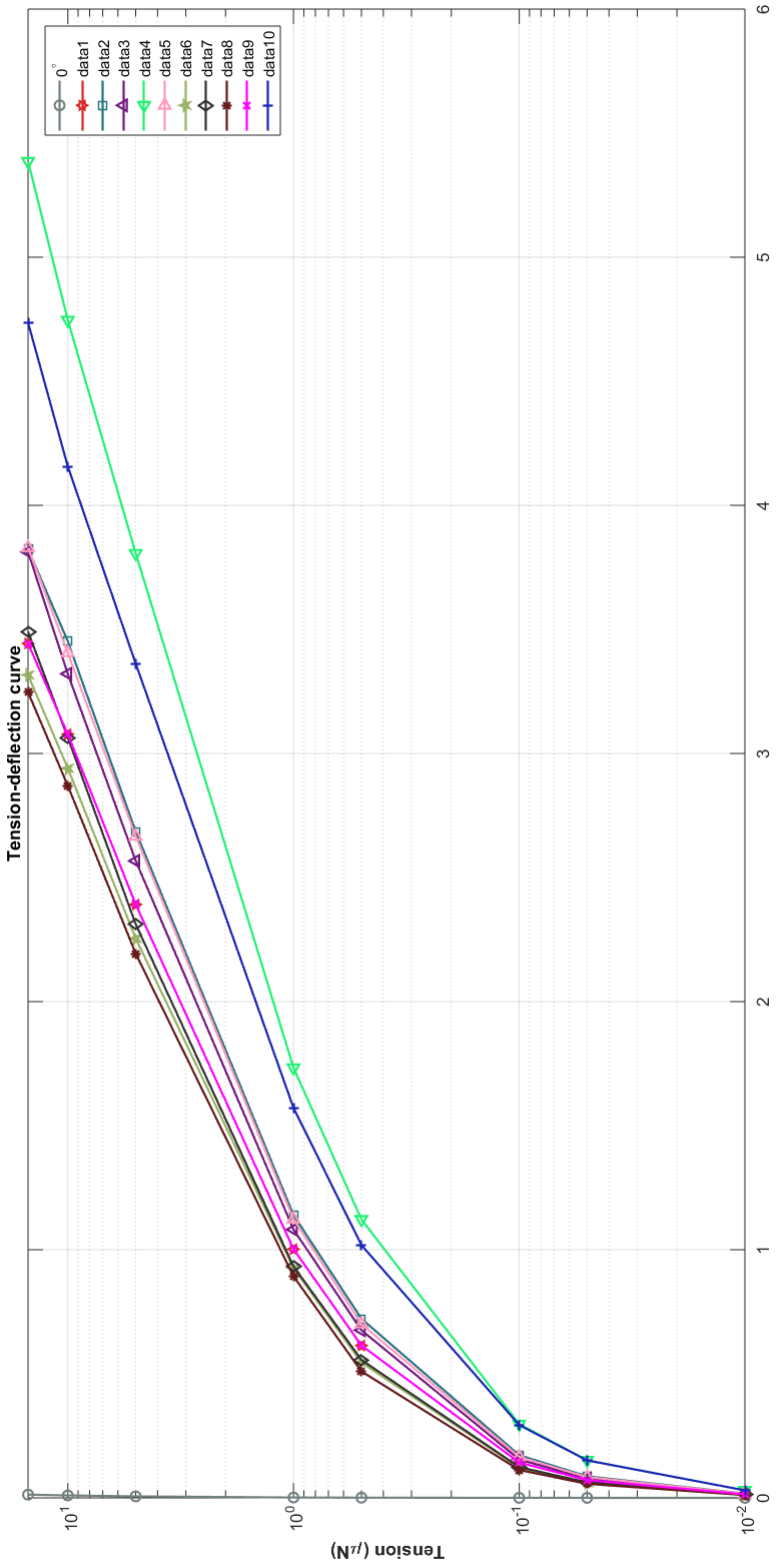

Figure 4.11: Tension-deformation curves

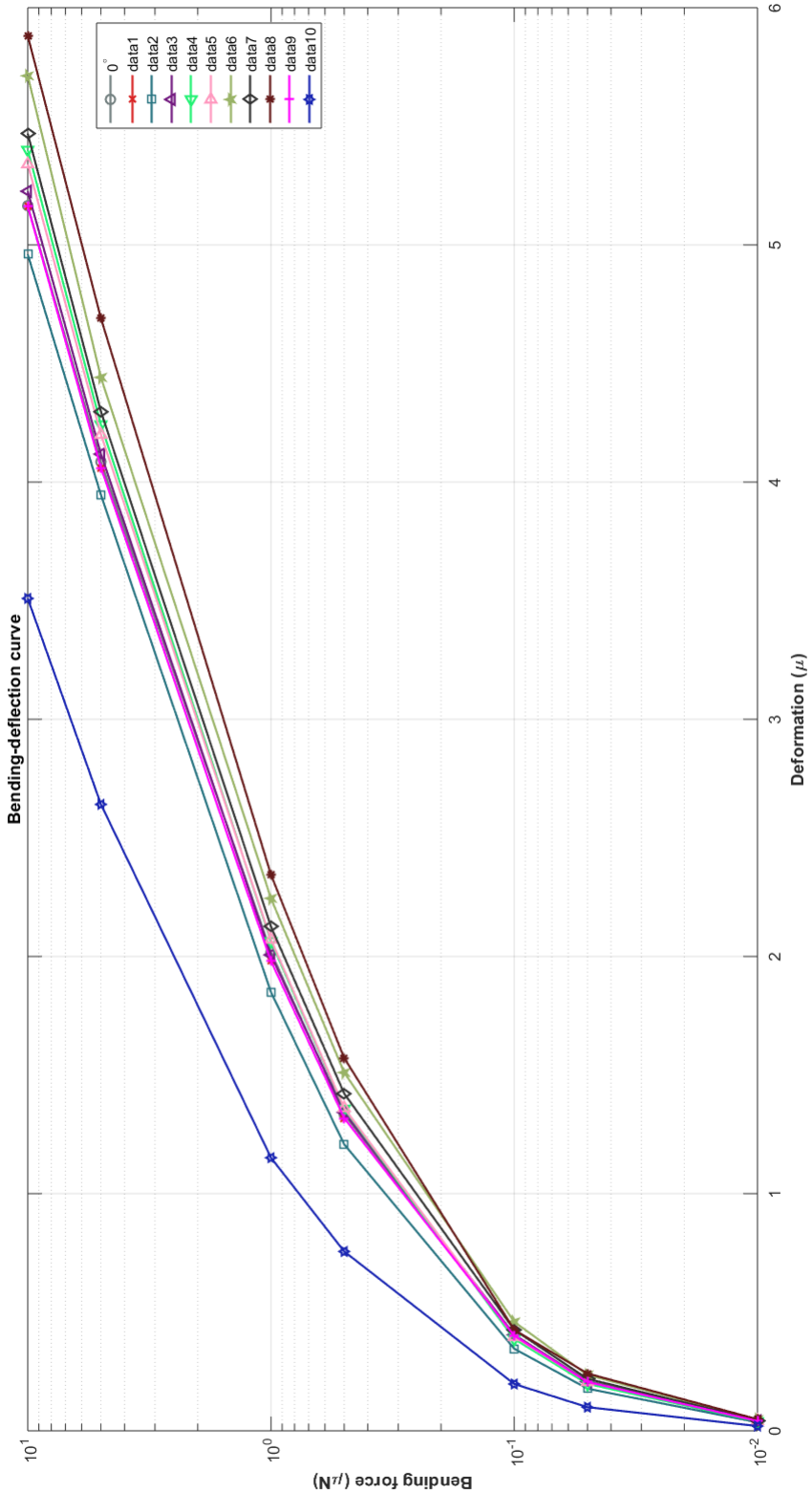

Figure 4.12: Bending-deflection curves

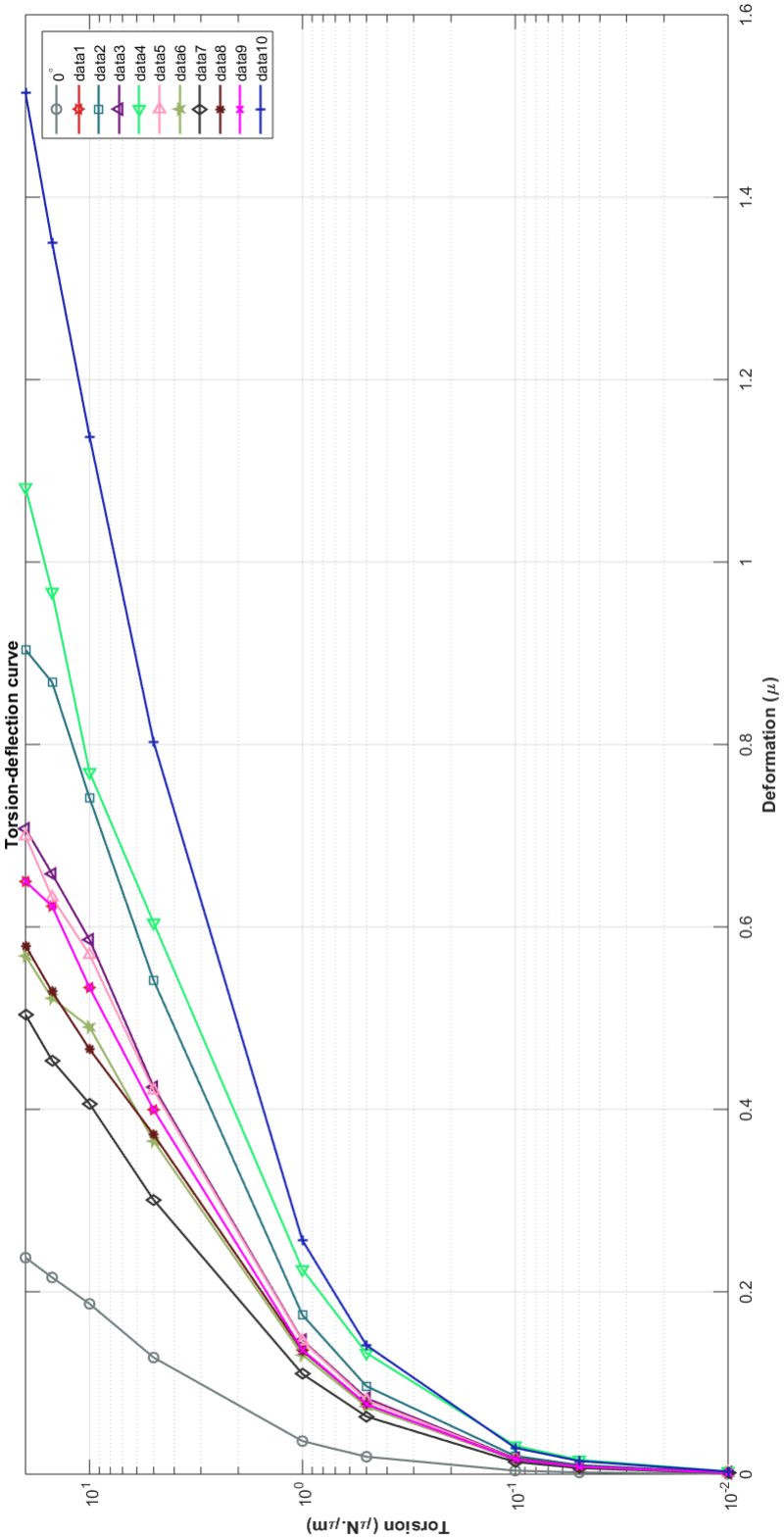

Figure 4.13: Torsion-deformation curves

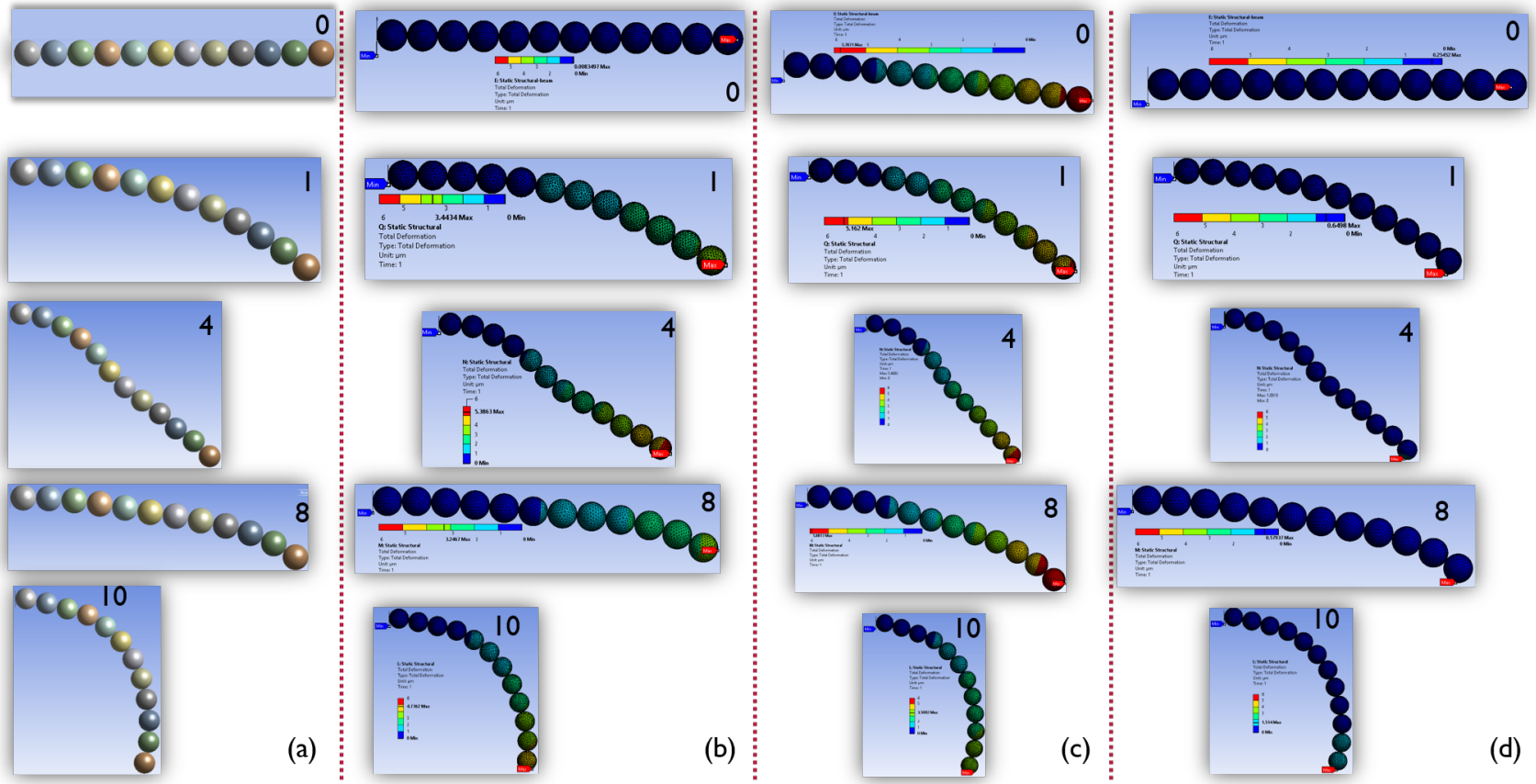

Figure 4.14: (a) Actual model; Distribution of deformation along the protofilament on application of (b) tensile force (c) bending force (d) torsional moment

4.5 Modal analysis of Protofilament structure

A free-free modal analysis is applied to the beam model of a single protofilament, as shown in Fig. 4.15 to observe the mode shapes formed, along with their respective frequencies. The material of the beam is the same as used in the structural analysis and is listed in Table 4.2.

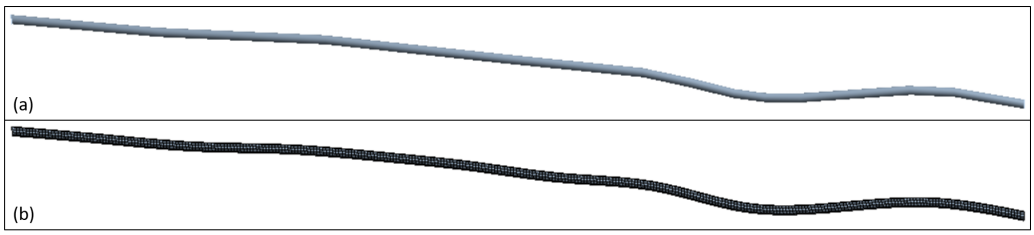

Figure 4.15: (a) Protofilament beam model; (b) Mesh: Min. element size = 0.4 μm

Results

The results of the modal analysis are shown in Fig. 4.16. From the plot, it is evidently clear that the frequencies of the mode shapes increase with an increase in the mode shape number. The first few mode shapes have a very low natural frequency when compared to the very high frequency values seen in higher mode shapes. It can be seen that all the different protofilament configurations follow a similar increasing trend in the frequencies with increasing mode shape numbers. This increasing trend is observed by the Civalek et al. [46] as well, where they performed free vibrational analysis on microtubule structures based on Differential Quadrature theory, with varying boundary conditions. The first three mode shapes occur at either zero or closer to zero frequencies and then starts to rise up. Thus, we can say that the first five mode shapes observed are trivial results. The zig-zag pattern observed in the mode shapes vs frequency graph, is similar to the observations made by Havelka et al. where they studied the deformation pattern of vibrating microtubules using an atomistic approach and determined that the tubulin-tubulin bond strength is vital for the mchanics of the MTs [48].

Table 4.6: Frequency values (MHz) for twelve mode shapes obtained from modal analysis

PF#	MS #1	MS #2	MS #3	MS #4	MS #5	MS #6	MS #7	MS #8	MS #9	MS #10	MS #11	MS #12
0	0	4.0Ee-06	1.47E-05	1.68E-05	0.000105	0.17118	0.17119	0.47170	0.47172	0.92426	0.9243	1.5268
1	0	7.54E-06	1.70E-05	0.20347	0.20351	0.56046	0.6087	1.0982	1.1065	1.8132	1.8143	2.7066
2	0	6.76E-06	1.19E-05	1.40E-05	1.86E-05	0.20285	0.20306	0.55871	0.64337	1.0946	1.1084	1.8067
3	0	0	1.15E-05	1.66E-05	1.96E-05	0.20274	0.23818	0.55804	0.63168	1.087	1.4018	1.7993
4	0	5.66E-06	8.85E-06	1.29E-05	0.20007	0.26118	0.54732	0.83839	1.0741	1.128	1.7371	1.9022
5	0	0	4.99E-06	1.09E-05	0.19546	0.2096	0.53567	0.84534	1.0546	1.0924	1.7368	1.8921
6	0	2.39E-06	8.49E-06	1.06E-05	0.2033	0.20335	0.55928	0.58154	1.0874	1.3664	1.8082	1.811
7	0	0	5.46E-06	8.01E-06	1.21E-05	0.20337	0.29044	0.56058	0.56432	1.0975	1.1256	1.8128
8	0	0	1.19E-05	1.35E-05	1.66E-05	0.20311	0.24105	0.55838	0.79885	1.0956	1.1221	1.8074
9	0	7.81E-06	1.01E-05	1.54E-05	1.68E-05	2.41E-05	0.20282	0.25993	0.55905	0.56843	1.0941	1.1707
10	0	6.10E-06	8.45E-06	1.32E-05	1.35E-05	0.19814	0.20151	0.54282	0.70066	1.0615	1.2416	1.7613

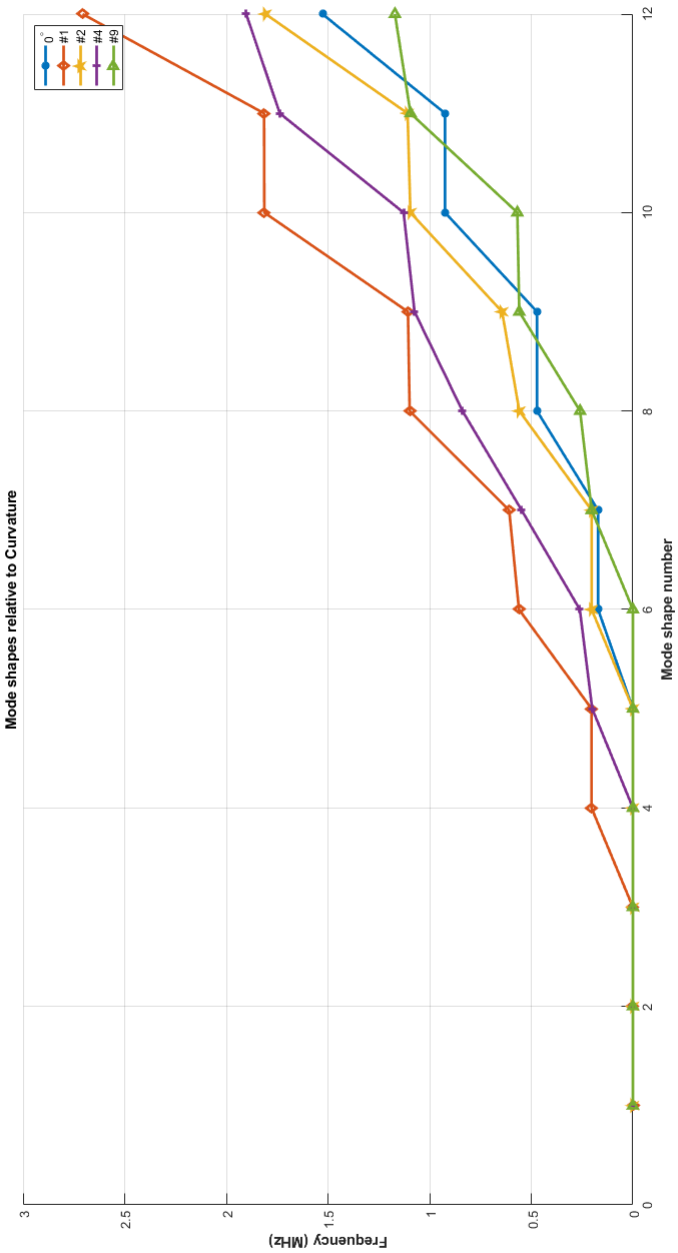

Figure 4.16: Mode shape results for 5 protofilament beam models

Chapter 5

Conclusions and Future Work

A self assembly study was conducted to observe the dynamic self assembly of protofilament structures in a microtubule, by running experiments manually in a lab, with the help of a vibration shaker. Ten most commonly occurring protofilament configurations were identified and contrasted with results obtained from physics simulations designed in Unity. On comparison, the results from the simulations show a high similarity with the experimental results, based on the type of protofilament structures observed. This provides us with an alternative approach to studying self organization in complex systems, keeping in mind the physical and financial constraints associated with conducting experiments specifically in biological systems. A mesh convergence study was carried out on the FEM model of a straight protofilament configuration, to verify that the optimal minimum element size for the geometric mesh is 0.4 μm. The response of the ten commonly occurring configurations along with the straight protofilament configuration, to different loading conditions like bending, tension and torsional loading were observed in this study, and a common trend where small curvatures do not affect the deformation values of the protofilaments was detected. The deformation under loading on the protofilament structure follows the deflections observed in cantilever beams, as the value increases progressively from the fixed end to the free end.

However, we were not equipped to conclude on the effects of curvature on the vibrational properties of the protofilaments, as the mode shapes obtained do not show a clear relationship. But we were able to determine that higher mode shapes vibrate at higher frequencies and there was an exponential increase in the frequency after the first few mode shapes which vibrated at extremely low frequencies.

Future Work

There is a lot of scope to further research in the self organization in microtubules by experimenting with different shapes like wedge shaped dimers, instead of the spherical shaped units used in this thesis. The rules of self assembly needs to be extended from the protofilament structures, to the formation of rings and whole microtubule structures. We plan to advance the FEM model to a ring structure, and analyze it's structural properties when bending, tension and torsional loading are applied. The FEM model is also extended to the microtubule structure as a whole to study it's load bearing capacity and the influence of curvature. Also, as the microtubules act as carriers for MAPs to walk on, there are loads acting along the length of the microtubule. We plan to analyze the effect of these induced stresses on the MT structure.

Bibliography

[1] 2015. [Online]. Available: https://www.nia.nih.gov/health/alzheimers-disease-fact-sheet#causes

[2] 02/09/2015 2016. [Online]. Available: https://www.cancer.gov/about-cancer/understanding/what-is-cancer

[3] D. C. Jean and P. W. Baas, "It cuts two ways: microtubule loss during alzheimer disease," *The EMBO Journal*, vol. 32, no. 22, pp. 2900–2902, 2013. [Online]. Available: http://www.ncbi.nlm.nih.gov/pmc/articles/PMC3831311/

[4] A. L. Parker, M. Kavallaris, and J. A. McCarroll, "Microtubules and their role in cellular stress in cancer," *Frontiers in Oncology*, vol. 4, p. 153, 2014. [Online]. Available: http://www.ncbi.nlm.nih.gov/pmc/articles/PMC4061531/

[5] G. M. Whitesides and B. Grzybowski, "Self-assembly at all scales," *Science*, vol. 295, no. 5564, p. 2418, 2002. [Online]. Available: http://science.sciencemag.org/content/295/5564/2418.abstract

[6] S. Zhang, "Emerging biological materials through molecular self-assembly," *Biotechnology Advances*, vol. 20, no. 5, pp. 321–339, 2002. [Online]. Available: http://www.sciencedirect.com/science/article/pii/S0734975002000265

[7] A. Aggarwal, S. Cheng, S. Cheng, M. J. Stevens, and A. Aggarwal, "Self-assembly of artificial microtubules," *SOFT MATTER*, vol. 8, no. 20, pp. 5666–5678, 2012. [Online]. Available: http://proxy-remote.galib.uga.edu/login?url=http://search.ebscohost.com/login.aspx?direct=true&db=edswsc&AN=000303998700031&site=eds-live

[8] 2009. [Online]. Available: https://www.britannica.com/science/cytoskeleton

[9] T. Mitchison and M. Kirschner, "Microtubule assembly nucleated by isolated centrosomes," *Nature*, vol. 312, no. 5991, p. 232, 1984.

[10] D. Chretien and R. H. Wade, "New data on the microtubule surface lattice," *Biology of the Cell*, vol. 71, no. 1-2, pp. 161–174, 1991. [Online]. Available: http://dx.doi.org/10.1016/0248-4900(91)90062-R

[11] G. Fink and C. H. S. Aylett, *Tubulin-Like Proteins in Prokaryotic DNA Positioning*. Cham: Springer International Publishing, 2017, pp. 323–356. [Online]. Available: https://doi.org/10.1007/978-3-319-53047-5_11

[12] Z. Zhao, H. Liu, Y. Luo, S. Zhou, L. An, C. Wang, Q. Jin, M. Zhou, and J.-R. Xu, "Molecular evolution and functional divergence of tubulin superfamily in the fungal tree of life," *Scientific Reports*, vol. 4, p. 6746, 2014. [Online]. Available: http://dx.doi.org/10.1038/srep06746

[13] Y. F. Inclan and E. Nogales, "Structural models for the self-assembly and microtubule interactions of gamma-, delta- and epsilon-tubulin," *Journal of Cell Science*, vol. 114, no. 2, p. 413, 2001. [Online]. Available: http://jcs.biologists.org/content/114/2/413.abstract

[14] A. B. Harvey Lodish and S. L. Z. et al, *Molecular Cell Biology (4th edition)*, ser. Biochemistry and Molecular Biology Education. Elsevier, 2000, vol. 29. [Online]. Available: https://www.ncbi.nlm.nih.gov/books/NBK21580/

[15] G. M. Cooper and R. E. Hausman, *The cell : a molecular approach*, 5th ed. Washington, D.C. : Sunderland, Mass. :: ASM Press ; Sinauer Associates, 2009. [Online]. Available: https://www.ncbi.nlm.nih.gov/books/NBK9833/

[16] L. Cassimeris, J. C. Leung, and D. J. Odde, "Monte Carlo simulations of microtubule arrays: The critical roles of rescue transitions, the cell boundary, and tubulin

concentration in shaping microtubule distributions," *PLOS ONE*, vol. 13, no. 5, p. e0197538, 2018. [Online]. Available: https://doi.org/10.1371/journal.pone.0197538

[17] M. Lenz and T. A. Witten, "Geometrical frustration yields fibre formation in self-assembly," *Nature Physics*, vol. 13, p. 1100, 2017. [Online]. Available: http://dx.doi.org/10.1038/nphys4184

[18] A. Papadopoulou, J. Laucks, and S. Tibbits, "From self-assembly to evolutionary structures," *Architectural Design*, vol. 87, no. 4, pp. 28–37, 2017. [Online]. Available: https://doi.org/10.1002/ad.2192

[19] M. Motamedi and M. M. Mashhadi, "Dynamic simulation and mechanical properties of microtubules," *Journal of Solid Mechanics Vol*, vol. 8, no. 4, pp. 781–787, 2016.

[20] S. Kasas, A. Kis, B. M. Riederer, L. Forró, G. Dietler, and S. Catsicas, "Mechanical properties of microtubules explored using the finite elements method," *ChemPhysChem*, vol. 5, no. 2, pp. 252–257, 2004. [Online]. Available: http://dx.doi.org/10.1002/cphc.200300799

[21] O. Civalek and C. Demir, "A simple mathematical model of microtubules surrounded by an elastic matrix by nonlocal finite element method," *Applied Mathematics and Computation*, vol. 289, no. Supplement C, pp. 335–352, 2016. [Online]. Available: http://www.sciencedirect.com/science/article/pii/S0096300316303435

[22] I. M. J'anosi, D. Chrétien, and H. Flyvbjerg, "Structural microtubule cap: stability, catastrophe, rescue, and third state," *Biophysical Journal*, vol. 83, no. 3, pp. 1317–1330, 2002. [Online]. Available: http://www.ncbi.nlm.nih.gov/pmc/articles/PMC1302230/

[23] A. Kis, S. Kasas, B. Babić, A. J. Kulik, W. Benoit, G. A. D. Briggs, C. Schönenberger, S. Catsicas, and L. Forró, "Nanomechanics of microtubules," *Physical Review Letters*, vol. 89, no. 24, p. 248101, 2002. [Online]. Available: https://link.aps.org/doi/10.1103/PhysRevLett.89.248101

[24] S. Yj, "Relevance of timoshenko-beam model to microtubules of low shear modulus," *Physica.*, vol. 41, no. 2, p. 213, 2008.

[25] D. B. Wells and A. Aksimentiev, "Mechanical properties of a complete microtubule revealed through molecular dynamics simulation," *Biophys J*, vol. 99, no. 2, pp. 629–37, 2010. [Online]. Available: https://www.ncbi.nlm.nih.gov/pubmed/20643083

[26] Z. Wu, E. Nogales, and J. Xing, "Comparative studies of microtubule mechanics with two competing models suggest functional roles of alternative tubulin lateral interactions," *Biophysical Journal*, vol. 102, no. 12, pp. 2687–2696, 2012. [Online]. Available: http://www.ncbi.nlm.nih.gov/pmc/articles/PMC3379015/

[27] E. Nogales, S. G. Wolf, and K. H. Downing, "Structure of the tubulin dimer by electron crystallography," *Nature*, vol. 391, p. 199, 1998. [Online]. Available: http://dx.doi.org/10.1038/34465

[28] Z. J. Donhauser, W. B. Jobs, and E. C. Binka, "Mechanics of microtubules: Effects of protofilament orientation," *Biophysical Journal*, vol. 99, no. 5, pp. 1668–1675, 2010. [Online]. Available: http://www.ncbi.nlm.nih.gov/pmc/articles/PMC2931733/

[29] M. I. Molodtsov, E. A. Ermakova, E. E. Shnol, E. L. Grishchuk, J. R. McIntosh, and F. I. Ataullakhanov, "A molecular-mechanical model of the microtubule," *Biophysical Journal*, vol. 88, no. 5, pp. 3167–3179, 2005. [Online]. Available: http://www.ncbi.nlm.nih.gov/pmc/articles/PMC1305467/

[30] S. Feng and H. Liang, "A coarse grain model of microtubules," *Theoretical and Applied Mechanics Letters*, vol. 2, no. 1, p. 014006, 2012. [Online]. Available: http://www.sciencedirect.com/science/article/pii/S2095034915301215

[31] A. Aggarwal, S. Cheng, S. Cheng, M. J. Stevens, and A. Aggarwal, "Self-assembly of artificial microtubules," *SOFT MATTER*, vol. 8, no. 20, pp. 5666–5678, 2012. [Online].

Available: http://proxy-remote.galib.uga.edu/login?url=http://search.ebscohost.com/login.aspx?direct=true&db=edswsc&AN=000303998700031&site=eds-live

[32] E. D. Spoerke, G. Bachand, D. Y. Sasaki, M. J. Stevens, J. Bollinger, B. H. Jones, J. S. Wheeler, J. Vervacke, A. Martinez, and D. McGrath, "Active assembly of dynamic and adaptable materials: Artificial microtubules," Sandia National Lab.(SNL-NM), Albuquerque, NM (United States), Report, 2017.

[33] P. Zakharov, N. Gudimchuk, V. Voevodin, A. Tikhonravov, F. I. Ataullakhanov, and E. L. Grishchuk, "Molecular and mechanical causes of microtubule catastrophe and aging," *Biophysical Journal*, vol. 109, no. 12, pp. 2574–2591, 2015. [Online]. Available: http://www.sciencedirect.com/science/article/pii/S000634951501156X

[34] O. V. S. Sarma, "A swarm engineering framework for microtubule self-organization," M.S thesis, 2017.

[35] S. P. Pearce, M. Heil, O. E. Jensen, G. W. Jones, and A. Prokop, "Curvature-sensitive kinesin binding can explain microtubule ring formation and reveals chaotic dynamics in a mathematical model," *arXiv preprint arXiv:1803.07312*, 2018.

[36] V. S. Vandelinder, "Biomolecular motors as nanofluidic transporters." Sandia National Lab.(SNL-NM), Albuquerque, NM (United States), Tech. Rep., 2017.

[37] I. M. Jnosi, D. Chrtien, and H. Flyvbjerg, "Modeling elastic properties of microtubule tips and walls," *European Biophysics Journal*, vol. 27, no. 5, pp. 501–513, 1998. [Online]. Available: https://doi.org/10.1007/s002490050160

[38] J. Zhang and C. Wang, "Molecular structural mechanics model for the mechanical properties of microtubules," *Biomechanics and Modeling in Mechanobiology*, vol. 13, no. 6, pp. 1175–1184, 2014. [Online]. Available: https://doi.org/10.1007/s10237-014-0564-x

[39] A. Shahinnejad, M. Haghpanahi, and F. Farmanzad, "Finite element analysis of axonal microtubule bundle under tension and torsion," *Procedia Engineering*, vol. 59,

pp. 16–24, 2013. [Online]. Available: http://www.sciencedirect.com/science/article/pii/S1877705813010023

[40] F. Gittes, B. Mickey, J. Nettleton, and J. Howard, "Flexural rigidity of microtubules and actin filaments measured from thermal fluctuations in shape," *The Journal of Cell Biology*, vol. 120, no. 4, pp. 923–934, 1993. [Online]. Available: http://www.ncbi.nlm.nih.gov/pmc/articles/PMC2200075/

[41] K. M. Liew, P. Xiang, and L. W. Zhang, "Mechanical properties and characteristics of microtubules: A review," *Composite Structures*, vol. 123, no. Supplement C, pp. 98–108, 2015. [Online]. Available: http://www.sciencedirect.com/science/article/pii/S026382231400676X

[42] A. Shamloo, F. Manuchehrfar, and H. Rafii-Tabar, "A viscoelastic model for axonal microtubule rupture," *Journal of Biomechanics*, vol. 48, no. 7, pp. 1241–1247, 2015. [Online]. Available: http://www.sciencedirect.com/science/article/pii/S0021929015001761

[43] M. Soheilypour, M. Peyro, S. J. Peter, and M. R. Mofrad, "Buckling behavior of individual and bundled microtubules," *Biophysical Journal*, vol. 108, no. 7, pp. 1718–1726, 2015. [Online]. Available: http://www.ncbi.nlm.nih.gov/pmc/articles/PMC4390818/

[44] C. Y. Wang, C. Q. Ru, and A. Mioduchowski, "Vibration of microtubules as orthotropic elastic shells," *Physica E: Low-dimensional Systems and Nanostructures*, vol. 35, no. 1, pp. 48–56, 2006. [Online]. Available: http://www.sciencedirect.com/science/article/pii/S1386947706003456

[45] S. Li, C. Wang, and P. Nithiarasu, "Structure property relation and relevance of beam theories for microtubules: a coupled molecular and continuum mechanics study,"

Biomechanics and Modeling in Mechanobiology, vol. 17, no. 2, pp. 339–349, 2018. [Online]. Available: https://doi.org/10.1007/s10237-017-0964-9

[46] Ö. Civalek and B. Akgöz, "Free vibration analysis of microtubules as cytoskeleton components: Nonlocal euler-bernoulli beam modeling," *Scientia Iranica. Transaction B, Mechanical Engineering*, vol. 17, no. 5, pp. 367–375, 2010.

[47] J. Kim, N. Li, R. Pidaparti, X. Wang, Y. Mao, C. Li, P. Ge, F. Wang, L. Wang, and S. Mondésert-Deveraux, "Microtubular protofilament analysis based on molecular level tubulin interaction," *Issues*, vol. 15, 2018.

[48] D. Havelka, M. A. Deriu, M. Cifra, and O. Kuera, "Deformation pattern in vibrating microtubule: Structural mechanics study based on an atomistic approach," *Scientific Reports*, vol. 7, no. 1, p. 4227, 2017. [Online]. Available: https://doi.org/10.1038/s41598-017-04272-w

Appendix A

Mathematical Notations

k_s: Axial spring constant

P: Load

L: Length of the structure

A: Cross - sectional area of the structure

E: Young's modulus

I: Moment of Inertia

T: Tension

M: Moment

δ: Deformation

Appendix B

Abbreviations

MT: Microtubule

MAP: Microtubule associated protein

MTOC: Microtubule organizing center

GTP: Guanosine triphosphate

GDP: Guanosine diphosphate

PF: Protofilament

FEA: Finite element analysis

FEM: Finite element modeling

ATP: Adenosine triphosphate

AFM: Atomic Force Microscope